Somatodendritic Targeting of M5 Muscarinic Receptor in the Rat Ventral Tegmental Area: Implications for Mesolimbic Dopamine Transmission

Miguel Garzón,[1,2,3]* and Virginia M. Pickel[3]

[1]Department of Anatomy, Histology, and Neuroscience, Medical School, Universidad Autónoma de Madrid (UAM), Madrid, 28029, Spain
[2]Research Institute, La Paz University Hospital (IDIPAZ), Madrid 28046, Spain
[3]Department of Neuroscience, Brain and Mind Research Institute, Weill Medical College of Cornell University, New York, New York 10065

ABSTRACT

Muscarinic modulation of mesolimbic dopaminergic neurons in the ventral tegmental area (VTA) plays an important role in reward, potentially mediated through the M5 muscarinic acetylcholine receptor (M5R). However, the key sites for M5R-mediated control of dopamine neurons within this region are still unknown. To address this question we examined the electron microscopic immunocytochemical localization of antipeptide antisera against M5R and the plasmalemmal dopamine transporter (DAT) in single sections through the rat VTA. M5R was located mainly to VTA somatodendritic profiles (71%; $n = 627$), at least one-third (33.2%; $n = 208$) of which also contained DAT. The M5R immunoreactivity was distributed along cytoplasmic tubulovesicular endomembrane systems in somata and large dendrites, but was more often located at plasmalemmal sites in small dendrites, the majority of which did not express DAT. The M5R-immunoreactive dendrites received a balanced input from unlabeled terminals forming either asymmetric or symmetric synapses. Compared with dendrites, M5R was less often seen in axon terminals, comprising only 10.8% ($n = 102$) of the total M5R-labeled profiles. These terminals were usually presynaptic to unlabeled dendrites, suggesting that M5R activation can indirectly modulate non–DAT-containing dendrites through presynaptic mechanisms. Our results provide the first ultrastructural evidence that in the VTA, M5R has a subcellular location conducive to major involvement in postsynaptic signaling in many dendrites, only some of which express DAT. These findings suggest that cognitive and rewarding effects ascribed to muscarinic activation in the VTA can primarily be credited to M5R activation at postsynaptic plasma membranes distinct from dopamine transport. J. Comp. Neurol. 521: 2927–2946, 2013.

INDEXING TERMS: motivation; reward; acetylcholine; reinforcement; ultrastructure

The midbrain ventral tegmental area (VTA) is the origin of the mesocorticolimbic projection system, which is highly involved in dopamine (DA)-mediated reward and motivated behaviors. DA-containing neurons of the VTA can be identified by the presence of the dopamine transporter (DAT), a carrier that reuptakes DA from the extracellular space to terminate neurotransmission, and also mediates calcium-independent DA local dendritic release by reversal of gradient (Nirenberg et al., 1997). In addition, DAT is the binding site for cocaine and other psychostimulants that are exogenous reinforcers of DA-related behaviors (Kuhar et al., 1991; Giros et al., 1996). The major involvement in psychostimulant reward is consistent with the preferentially high DAT expression in mesolimbic DA neurons that project to the nucleus acccumbens (NAc), compared with those

Grant sponsor: National Institute of Mental Health, National Institute of Health; Grant number: MH40342; Grant sponsor: National Institute of Health; Grant number: HL09657; Grant sponsor: National Institute of Drug Abuse; Grant number: DA04600, DA005130 (to V.M.P.). Grant sponsor: Ministerio de Ciencia e Innovacicen, Spain; Grant number: BFU2009-06991 (to M.G.).

*Correspondence to: Miguel Garzón, M. D., Ph. D., Department of Anatomy, Histology, and Neuroscience, Medical School UAM, Arzobispo Morcillo 4, Madrid 28029, Spain. E-mail: miguel.garzon@uam.es

Received December 10, 2012; Revised January 29, 2013;
Accepted for publication February 26, 2013.
DOI 10.1002/cne.23323
Published online March 16, 2013 in Wiley Online Library (wileyonlinelibrary.com)

projecting to the prefrontal cortex (Nirenberg et al., 1998; Sesack et al., 1998).

Cholinergic axon terminals, originating in the mesopontine cholinergic nuclei (Henderson and Sherriff, 1991; Oakman et al., 1995; Omelchenko and Sesack, 2005), establish synaptic contacts with dopaminergic neurons of the VTA (Garzón et al., 1999; Omelchenko and Sesack, 2006). Mesopontine cholinergic projections to the VTA modulate DA-related mesolimbic rewarding behaviors, such as self-administration of cocaine (Mark et al., 2011; You et al., 2011), amphetamine (Alderson et al., 2004), and heroin (Olmstead et al., 1998; Zhou et al., 2007). Further evidence for involvement of acetylcholine muscarinic receptors in the modulation of DA-mediated rewarding functions of VTA mesolimbic neurons is provided by the observed increase in DA release in the NAc after muscarinic VTA stimulation (Westerink et al., 1996; Gronier et al., 2000) or muscarinic disinhibition of mesopontine nuclei that provide cholinergic input to the VTA (Yeomans, 1995).

Peripheral administration of muscarinic agents modulates DA release in mesolimbic areas and also alters DA-related behaviors (Yeomans et al., 1993; Yeomans, 1995; Bymaster et al., 1998; Fink-Jensen et al., 1998). Likewise, the application of muscarinic agonists in the VTA increases both neuronal discharge rate within the VTA (Lacey et al., 1990; Gronier and Rasmussen, 1998) and DA release in the NAc (Westerink et al., 1996; Gronier et al., 2000). Furthermore, muscarinic receptors within the VTA regulate both basal (Miller and Blaha, 2005) and morphine-induced (Miller et al., 2005) DA release in the NAc. In addition, intra-VTA microinjection of muscarinic antagonists attenuates lever-pressing maintained by lateral hypothalamic stimulation reward (Yeomans and Baptista, 1997), and cocaine enhancement of laterodorsal tegmental nucleus (LDT) stimulation-evoked DA release in the NAc (Lester et al., 2010).

Muscarinic receptors are thought to be the main cholinergic receptors contributing to brain-stimulation reward, because muscarinic antagonists block brain-stimulation reward more efficiently than nicotinic antagonists in the VTA (Yeomans and Baptista, 1997). Both conditioned place preference and sef-administration paradigms have shown the rewarding effects of muscarinic agonists in the VTA (Ikemoto and Wise, 2002; Mark et al., 2011). Together, these observations suggest that dopaminergic neurons within the VTA that project to the NAc and other limbic brain regions are regulated by muscarinic ligands.

Five muscarinic receptor genes have been cloned (Kubo et al., 1986; Bonner et al., 1987, 1988; Peralta et al., 1987), and their protein receptors localized in the rat brain by light immunohistochemistry by using selective subtype-specific antibodies (Levey et al., 1991). In the VTA, the distribution of M2 receptor, which is involved in cognitive and goal-based DA-mediated behaviors, is mainly plasmalemmal in non-DA neurons, but is prominently cytoplasmic in DA neurons (Garzón and Pickel, 2006). The M5R subtype is the most recently cloned receptor of the muscarinic receptor family (Bonner et al., 1988; Liao et al., 1989), and also the one whose mRNA is confined almost exclusively to midbrain DA neurons within the VTA and substantia nigra, showing no detectable expression in other brain regions or in non-DA neurons (Weiner et al., 1990). In M5R-deficient (M5$-/-$) mice generated by gene targeting technology (Yamada et al., 2001; Bymaster et al., 2003; Wess, 2003), pharmacological and behavioral studies have shown an attenuation of the rewarding effects of psychostimulants and opiates (Basile et al., 2002; Fink-Jensen et al., 2003; Wang et al., 2004). Moreover, in contrast to wild-type animals, the M5$-/-$ mice do not show increased DA release in the limbic NAc after electrical stimulation of the mesopontine region known to contain the main cholinergic input to VTA mesocorticolimbic neurons (Forster and Blaha, 2000; Forster et al., 2002).

All these data support a critical role for M5R activation within the VTA in drug reinforcement and addictive behavior. Despite these relevant actions, the functional sites for activation of M5R in the VTA are still unknown and may include not only postsynaptic DA, but non-DA neurons or their afferent terminals. In the present study, we use high-resolution single- and dual-immunolabeling electron microscopy to 1) examine the subcellular localization of M5R in the VTA, and 2) determine whether DAT-containing dopaminergic VTA neurons, or their afferents, express the M5R.

MATERIALS AND METHODS

Antisera

We used a commercially available rat monoclonal antibody raised against DAT (MAB369, Chemicon, Temecula, CA) for the immunocytochemical labeling of dopaminergic cells in the VTA (Table 1). This antibody is directed against the N-terminus (residues 1–66) of the human DAT (Pristupa et al., 1994) fused to glutathione S-transferase (Ciliax et al., 1995). The specificity of the DAT antibody has been shown by 1) immunoblot analysis using cloned and native brain proteins (Hersch et al., 1997; Miller et al., 1997; Ciliax et al., 1999); or 2) western blot analysis of DAT fusion protein, without cross-reactivity to GST (Hersch et al., 1997). Additional characterization and specificity tests were done by immunoblotting using a stable SK-N-MC cell line expressing human DAT, untransfected SK-N-MC cells, and HeLa cells transiently expressing the human serotonin or norepinephrine

TABLE 1.
Primary Antibodies Used

Antigen	Immunogen	Manufacturer data	Raised in
M5R	Recombinant protein corresponding to amino acids 230–426 mapping within an internal region (i3) of muscarinic acetylcholine receptor M5 of human origin	Santa Cruz (sc-9110 [H-197])	Rabbit polyclonal
DAT	N-terminus (residues 1–66) of the human DAT fused to glutathione-S-transferase	Chemicon (AB369)	Rat monoclonal

DAT, dopamine transporter; M5R, M5 muscarinic receptor.

transporters. In these experiments, the DAT antibody recognized a single protein band of 85 kDa in the stable SKN-MC cell line expressing DAT (Hersch et al., 1997; Miller et al., 1997), with no cross-reactivity to the serotonin or norepinephrine transporters (Miller et al., 1997). Thus, in rat brain membranes, the DAT antibody binds to a single protein band with the same mobility as the cloned transporter (Hersch et al., 1997).

The specificity of the DAT antibody was also characterized by immunohistochemistry in brain tissue (Hersch et al., 1997; Ciliax et al., 1999). The distribution of the DAT antibody in rat brain agreed with known dopaminergic cell groups and their projections, and was identical to the distribution observed using polyclonal antibodies (Ciliax et al., 1995). Moreover, specificity of this antibody for DAT has also been tested by immunostaining brain sections from rat and monkey that received unilateral nigrostriatal lesions with 6-hydroxydopamine and 1-methyl-4-phenyl-1,2,3,6-tetrahydropyridine (MPTP), respectively (Hersch et al., 1997; Ciliax et al., 1999). Those neurotoxic lesions completely abolished DAT immunoreactivity in striatal regions ipsilateral to the lesion (Hersch et al., 1997; Ciliax et al., 1999).

The M5R immunoreactivity was detected with a rabbit polyclonal antiserum (Table 1) (sc-9110 [H-197], Santa Cruz Biotechnology, Santa Cruz, CA) directed against a recombinant protein corresponding to amino acids 230–426, forming part of the i3 intracellular loop of human m5 mAchR (Bonner et al., 1987; Peralta et al., 1987; Liao et al., 1989; Levey et al., 1991). The identity of the recombinant protein was confirmed by DNA sequence and sodium dodecyl sulfate-polyacrylamide gel electrophoresis (SDS-PAGE) western blotting of human cell lines (Liu et al., 2007b). This antiserum has also been characterized by western blot analysis in human fibroblasts, in which it recognized a protein of 95 kDa (Qu et al., 2006), by immunoprecipitation, and by immunocytochemistry. As controls for selective recognition of the M5R, sections through the VTA of two M5R knockout (Yamada et al., 2001) and two adult wild-type mice were examined for immunoperoxidase labeling by using the M5R antiserum. The null mice were adult (3 weeks) males (129/S6, CF1-M5R stock no. 1261) supplied by Taconic Farms (Germantown, NY). The observed presence of M5R immunolabeling in wild-type mice, but not in M5R knockout mice, is consistent with specificity of the antiserum for the M5R. In addition, we also tested specificity for secondary antisera under our particular experimental conditions in control experiments by replacing the M5R and the DAT antisera with normal sera, which produced no detectable labeling.

Animals

Six (250–300 g) male Sprague-Dawley rats (Taconic Farms) were deeply anesthetized with 150 mg/kg i.p. sodium pentobarbital. All efforts were made to minimize animal suffering, and to use the minimum necessary number of animals. The experimental protocol conformed strictly with National Institutes of Health guidelines for the Care and Use of Laboratory Animals and was approved by the Institutional Animal Care and Use Committee of Joan and Sanford I. Weill Medical College and Graduate School of Medical Sciences of Cornell University. Preparation of the tissue prior to immunocytochemistry was done according to procedures described by Leranth and Pickel (1989). The brains of the anesthetized rats were fixed by sequential aortic arch perfusion with: 1) 20 ml of heparin (1,000 U/ml) in saline; 2) 50 ml of 3.8% acrolein (Polysciences, Warrington, PA) in a solution of 2% paraformaldehyde in 0.1 M phosphate buffer, pH 7.4 (PB); and 3) 200 ml of 2% paraformaldehyde in 0.1 M PB. Four C57 BL6 mice (Taconic Farms), two of which had deletion of the M5R gene, were used for immunolabeling specificity control experiments. These were anesthetized and perfused by using a protocol similar to that of the rats. The exceptions in mice include perfusion through the left ventricle of the heart, and reduction of the volume of acrolein to 20 ml and the 2% paraformaldehyde to 100 ml.

Both rat and mouse brains were removed from the skull, dissected, cut into coronal blocks of 5–6 mm, and postfixed for 30 minutes in 2% paraformaldehyde in 0.1 M PB. Coronal sections were collected through the midbrain region including the VTA. These were cut at

40–50 μm thickness into 0.1 M PB at 4°C on a Leica Vibratome VT1000 S (Leica Instruments, Nussloch, Germany). The free-floating sections of tissue were incubated for 30 minutes in a solution of 1% sodium borohydride in 0.1 M PB to remove excess of active aldehydes (Eldred et al., 1983), and rinsed in 0.1 M PB until bubbles disappeared. To enhance the penetration of immunoreagents, the sections were then treated with the freeze-thaw technique, consisting of: 1) cryoprotection for 15 minutes in a solution of 25% sucrose and 3% glycerol in 0.05 M PB; 2) quick freezing in liquid chlorodifluoromethane (Freon, Refron, NY) followed by liquid nitrogen; and 3) thawing in 0.1 M PB at room temperature. After extensive rinsing in 0.1 M Tris-buffered saline, pH 7.6 (TS), the sections were incubated for 30 minutes in 0.5% bovine serum albumin (BSA) in 0.1 M TS to minimize nonspecific staining, and then processed for single- or dual-immunocytochemical labeling.

Immunocytochemistry

For single-labeling experiments with the M5R antiserum, tissue sections from three rats prepared as described above were incubated for 40 hours at 4°C in primary antiserum (1:2,000 for immunoperoxidase or 1:200 for immunogold). For immunoperoxidase detection of M5R, sections were incubated in: 1) biotinylated goat anti-rabbit IgG (1:400; Vector, Burlingame, CA) for 30 minutes; and 2) avidin–biotin complex (1:100) (Hsu et al., 1981) for another 30 minutes. The immunoreactivity bound to the tissue was visualized by a 6-minute incubation in 0.022% 3,3′-diaminobenzidine (Aldrich, St. Louis, MO) and 0.003% hydrogen peroxide in 0.1 M TS. All the incubations were carried out at room temperature (unless otherwise noted) with continuous agitation on a rotator and were followed by several rinses in 0.1 M TS between incubations.

For single immunogold detection of M5R, after the incubation in the primary antiserum as indicated above, tissue sections were transferred to 0.01 M phosphate-buffered saline, pH 7.4 (PBS), blocked for 10 minutes in 0.8% BSA and 0.1% gelatin in 0.01 M PBS, and incubated for 2 hours in colloidal gold (1 nm)-labeled goat anti-rabbit IgG, (1:50; Amersham, Arlington Heights, IL). After this, the sections were fixed for 10 minutes in 2% glutaraldehyde in 0.01 M PBS to enhance the adherence of the bound gold to the tissue, and reacted with a silver solution IntenSE M kit (Amersham) for either: 1) 4–6 minutes for electron microscopy; or 2) 8–10 minutes for light microscopy.

For dual-labeling experiments, tissue sections from four rats were incubated in a cocktail solution containing the M5R antiserum (1:200) and the antibody against DAT (1:20,000). The method of Chan et al. (1990) was used for pre-embedding immunoperoxidase and immunogold dual-labeling of the tissue. Thus, the immunoperoxidase reaction for DAT was followed by immunogold–silver detection of M5R, because the immunogold method gives a more precise subcellular localization of the receptors than the immunoperoxidase method. The primary antisera against M5R and DAT were raised in rabbits and rats, respectively, and therefore could be recognized by appropriate species-specific secondary antibodies. All the incubations were carried out at room temperature with continuous agitation on a rotator and were followed by several rinses in 0.1 M TS, 0.1 M PB, and 0.01 M PBS. In brief, the incubation in primary antisera was followed by incubation in secondary biotinylated goat anti-rat IgG (1:400; Chemicon) for 30 minutes and then in avidin–biotin–peroxidase complex (1:100, Vectastain Elite Kit, Vector) for another 30 minutes. Visualization of the peroxidase reaction product was achieved by revealing the tissue for 6 minutes in 0.022% 3,3′-diaminobenzidine and 0.003% hydrogen peroxide in 0.1 M TS. After this, the sections were rinsed in 0.1 M TS, transferred to 0.01 M PBS, and processed for M5R-immunogold labeling as described above for single-immunogold labeling.

Sections processed for light microscopy were rinsed in 0.05 M PB and mounted on glass slides. After overnight drying in a dessicator, they were dehydrated through immersion in a series of increasing-concentration alcohols, and defatted in xylene (J.T. Baker, Phillipsburg, NJ). Finally, the slides were coverslipped and examined in a Nikon microscope by using differential interference contrast optics.

Electron microscopy

Immunolabeled sections for electron microscopy were postfixed in 2% osmium tetroxide in 0.1 M PB for 1 hour, dehydrated through a series of graded ethanols and propylene oxide, and incubated overnight in a 1:1 mixture of propylene oxide and Epon (EMbed-812; Electron Microscopy Sciences, Fort Washington, PA). The sections were transferred to 100% Epon for 2 hours and flat-embedded in Epon between two sheets of Aclar plastic (Allied Signal, Pottsville, PA). Ultrathin sections (50–60 nm) were cut from the outer surface of the tissue with a diamond knife (Diatome, Fort Washington, PA) by using an ultramicrotome (Ultratome, NOVA; LKB-Productor, Bromma, Sweden). The regions examined were located in the VTA at the levels of anteroposterior planes −5.2 to −5.6 mm from Bregma of the rat brain atlas of Paxinos and Watson (1986). The sections were collected on 400-mesh copper grids, counterstained with uranyl acetate and lead citrate (Reynolds, 1963),

and, once completely dried, examined at 60 kV with a Tecnai Biotwin 12 (Serial # D271) transmission electron microscope (FEI, Hilsboro, OR).

Data analysis

Only sections near the surface of the tissue at the Epon–tissue interface were examined in order to ensure that the analysis was restricted to areas with optimal penetration of immunolabeling reagents. This procedure also helped to minimize biases in detecting immunoreactivity more frequently in large versus small profiles. The classification of identified cellular elements was based on the descriptions of Peters et al. (1991). Axon terminals were identified by the presence of numerous synaptic vesicles and were at least 0.2 μm in diameter. Small unmyelinated axons were $<$0.2 μm and rarely contained small vesicles. Neuronal somata were identified by the presence of a nucleus, Golgi apparatus, and rough endoplasmic reticulum. Dendrites usually contained abundant endoplasmic reticulum, and were distinguished from unmyelinated axons by their larger diameter and/or abundance of uniformly distributed microtubules. In addition, dendrites were in many cases postsynaptic to axon terminals. Asymmetric synapses were recognized by thick postsynaptic densities (asymmetric synapses, type Gray I), whereas symmetric synapses had thin pre- and postsynaptic specializations (symmetric synapses, type Gray II) (Gray, 1959). Zones of closely spaced parallel plasma membranes, which lacked discernible synaptic densities, but were otherwise not separated by glial processes, were defined as appositions or nonsynaptic contacts, and were not included in the quantification unless specifically stated. A profile was considered to be selectively immunoperoxidase labeled when it contained cytoplasmic precipitates making it appear more electron dense than morphologically similar profiles located within the same section. A profile was considered to contain immunogold labeling when two or more gold particles were observed within large profiles or when a single particle was seen in small profiles, such as unmyelinated small axons or narrow glial leaflets. For evaluation of the distribution of M5R in single M5R-immunoperoxidase or M5R-immunogold labelings, three Vibratome sections were used for each marker. The level of background (nonspecific) labeling was established by examining the resin and tissue areas that were not expected to express either DAT or M5R. Neither immunoperoxidase nor immunogold–silver labeling was observed in Epon regions without tissue or seen in myelinated sheaths of axons. Thus, quantitative analysis was not corrected for either immunoperoxidase or immunogold–silver background labeling.

The relationship between M5R- and DAT-labeled profiles was analyzed on the basis of electron micrographs containing both M5R and DAT immunoreactivity. Counting the same labeled structure twice was avoided by a systematic scanning of the surface of only one or two ultrathin sections that were separated by at least 700 nm in each of the individual Vibratome sections.

The ultrastructural quantitative analysis was carried out in 14 vibratome sections from four animals. The sections contained M5R-immunogold and DAT-immunoperoxidase labeling. All immunoreactive processes (n = 2,288) were counted in randomly sampled electron micrographs at magnifications of 9,300–23,000× from an area of 14,479.6 μm^2, with an area of at least 2,654.6 μm^2 examined in each of four animals. The tissue was quantitatively examined to determine the relative frequencies with which the immunoreactive products were localized within neuronal somata, dendrites, axons, or glial cells. In addition, morphologically recognizable synaptic relationships of each labeled profile were also quantified. Analyses of variance (ANOVAs) were used to determine whether there was significant variability in total labeled profiles per square micron of analyzed surface (area density) or in distribution of immunolabeling in different profile types with respect to different animals. Variations in the density of asymmetric and symmetric synapses established by either M5R-immunolabeled terminals or M5R-immunoreactive dendrites were assesed by using Student's t-tests.

An analysis of the ultrastructural distribution of M5R was carried out to ascertain: 1) the prevalence of M5R in association with specific cellular structures; and 2) the relationship between M5R- and DAT-immunolabeled profiles. The prevalence of different profile types (i.e., dendrites vs. axons, etc.) containing M5R was expressed as a percentage of all M5R-labeled elements. These M5R-labeled profiles were assessed from three to four Vibratome sections from each of four animals (n = 14). The tissue processed for immunogold–silver detection of M5R and immunoperoxidase labeling of DAT was also used for the examination of the relative number of gold–silver particles in association with either the plasma membrane or the cytoplasm of the M5R-immunogold–labeled dendrites. A particle was considered to be associated with the plasma membrane when any point of its contour was in contact with the plasma membrane. Assessment of the immunogold distribution of M5R was based on 1,597 gold–silver particles within 627 dendrites and on 197 gold–silver particles within 102 axon terminals. In dually labeled tissue sections, the cellular relationship between M5R- and DAT-labeled profiles was assessed for all contacts/colocalizations between respectively immunoreactive profiles. Because the animals were rather homogeneous in their patterns of immunolabeling

density and distribution, as well as in cellular associations of M5R-labeled profiles, we pooled data from different animals in the following descriptive analysis.

The electron micrographs used for the figures were acquired with an AMT digital camera (Advanced Microscopy Techniques, Danvers, MA) on a Microsmart Computer using a Windows 2000 operating system. To build and label the composite illustrations, Adobe Photoshop (version 7.0; Adobe Systems, Mountain View, CA) and Canvas (version 8.0.4; Deneba Systems, ACD Systems, Miami, FL) software programs were utilized for adjustment of brightness and contrast of the digital images. The images were then imported into PowerPoint to add the lettering and make the composite plate illustrations.

RESULTS

Light microscopic control studies in the rat VTA show intense M5R immunoperoxidase labeling in many putative neuronal profiles (Fig. 1A), which was absent when the primary anti-M5R antibody incubation was omitted from the immunohistochemical protocol (data not shown). The M5R distribution was comparable, but less robust than that seen with DAT immunolabeling. M5R immunoreactivity within the VTA of wild-type mice (Fig. 1B) had a similar pattern, although of lower intensity, to that observed in normal rats and was not seen in M5R knockout mice (Fig. 1C). The lower intensity of M5R immunoreactivity in wild-type mice compared with that seen in rats may reflect species-specific variations in M5R expression or methodological differences in perfusion fixation.

Electron microscopy established a primary localization of M5R immunoreactivity in somatodendritic profiles within the VTA, but also revealed the presence of labeling in axonal and glial profiles (Table 2). Compared with immunogold, the high sensitivity of the immunoperoxidase method allowed detection of M5R immunoreactivity in more of the small profiles, but lacked the resolution for subcellular distribution of M5R. However, there were no apparent differences in frequencies or types of associations between differentially labeled profiles. Therefore, for the subsequent statistical analysis, we used numbers obtained from the dual-labeled tissue in which M5R was detected with the immunogold method and DAT was detected with the immunoperoxidase method. Illustrations are, however, shown with these markers, as well as the reverse markers.

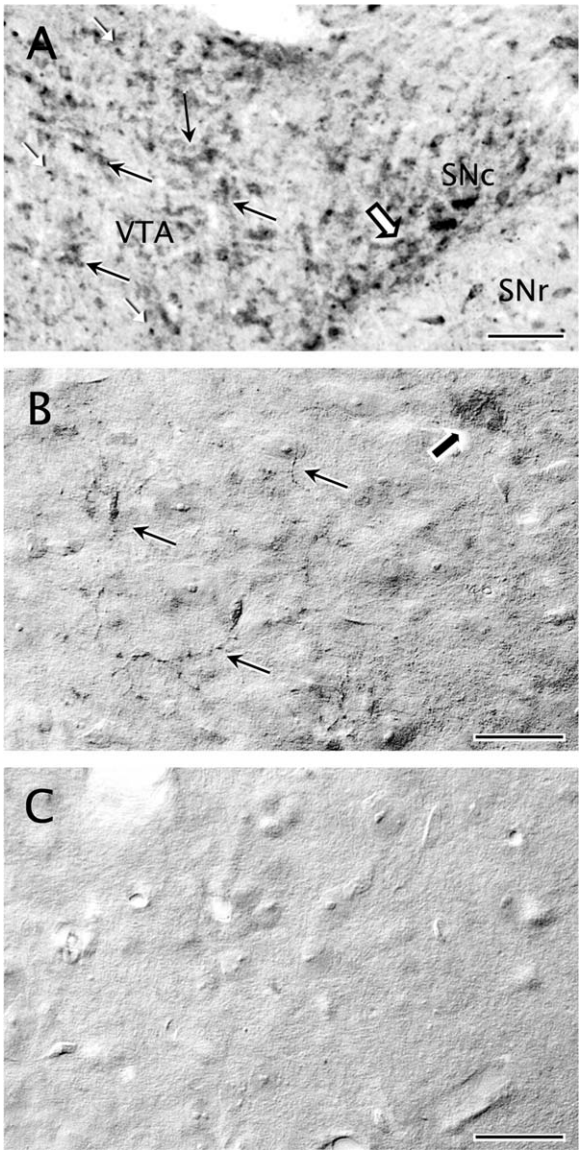

Figure 1. Specific M5 immunoreactivity is expressed in the ventral tegmental area (VTA). **A:** Distribution of M5 immunoreactivity in the neuropil of a wild-type rat midbrain section at −5.60 mm AP level from Bregma, as indicated in the Paxinos and Watson atlas (1986). Moderate immunoreaction is observed in profiles resembling neuronal somata and continuous dendrites in the VTA (black arrows) and in the adjacent substantia nigra compacta (SN; block arrow). A denser immunoreaction product is seen throughout the neuropil as punctate deposit in thin neuritic processes (white arrowheads). **B:** Distribution of M5 immunoreactivity in the neuropil of a wild-type mouse VTA. Light M5 immunolabeling is observed in the VTA, detected diffusely in some neuronal somata (block arrow) and also in thin varicose punctate processes that may be axons, as was the case for rats (A). **C:** Similar immunohistochemical processing in tissue sections collected at the same AP level as in B of an M5 null mouse shows no detectable M5 immunoreactivity. Scale bar = 25 μm in A–C.

M5R immunoreactivity in dendrites and somata

Over 70% of all M5R-labeled profiles were dendrites (627/868; Table 2). The majority of these dendrites were 0.5–2.5 μm in diameter. The dendritic M5R was mainly localized within the cytoplasm on and near plasma membranes contacted by unlabeled axon

TABLE 2.

Neuronal Distribution of M5- and/or DAT-Immunolabeled Cellular Profiles in the Rat VTA[a]

	Labeling								
	Total M5	Single M5		Dual DAT+M5			Single DAT		Total DAT
Type of cellular profile	No. of profiles	% from total M5	No. of profiles	% from total M5	No. of profiles	% from total DAT	No. of profiles	% from total DAT	No. of profiles
Dendrites	627	66.8	419	33.2	208	14.4	1,238	85.6	1,446
Somata	44	70.5	31	29.5	13	92.9	1	7.1	14
Axon terminals	102	96.1	98	3.9	4	14.3	24	85.7	28
Unmyelinated axons	88	98.9	87	1.1	1	1.4	73	98.6	74
Myelinated axons	7	100	7	0	0	–	0	–	0
Total	868	74.0	642	26.0	226	14.5	1,336	85.5	1,562

[a]Immunolabelings for M5 and/or DAT in different neuronal compartments within the rat VTA. Profiles containing single M5, single DAT, and dual DAT+M5 labelings are given as raw numbers and as percentage of the total M5- and/or total DAT-immunolabeled profiles in each category. Data were collected from 14 Vibratome sections in four rats processed for dual labeling. Labeling in glia and in profiles not clearly distinguished as neuronal or glial is not included in the table.

terminals (Fig. 2A,B). Aggregates of M5R-immunoperoxide (Fig. 2A) or -immunogold particles (Fig. 2B) were often localized beneath synaptic inputs from unlabeled terminals forming either symmetric (Fig. 2A) or asymmetric (Fig. 2B) junctions. In some cases, the M5R-immunogold was localized to the postsynaptic membrane specialization (Fig. 2B). In the immunogold–silver M5R-labeled sections, the number of gold–silver particles identifying M5R within the cytoplasm was greater than those in contact with the plasma membrane in dendrites (1,127 vs. 470). In most cases, the intracytoplasmic M5R-immunogold particles were distributed throughout the cytoplasm, and were often associated with endomembranes or tubulovesicles of the smooth endoplasmic reticulum in dendrites, some of which contained DAT immunolabeling (Fig. 2C).

M5R-immunoreactive somata comprised around 5% of the total M5R-labeled profiles in the VTA ($n = 44$ of 868; Table 2). In neuronal somata, M5R immunolabeling was primarily associated with cytoplasmic rather than plasma membranes (Fig. 3). Intense M5R labeling was observed in cisterns or saccules of the endoplasmic reticulum (Fig. 3B–D), lamellae of the Golgi complex, and endosome-like bodies (Fig. 3A). Although less frequent, M5R immunolabeling was also detected along the plasma membranes of some of the labeled perikarya (Fig. 3C,E). The segments of the plasmalemma in contact with gold–silver particles usually apposed axon terminals (Fig. 3E) or astrocytic expansions (Fig. 3C). The M5R-labeled somata were also contacted by either unlabeled or M5R-labeled terminals (Fig. 3E) and more rarely received synapses of the symmetric type ($n = 11$). From all M5R-labeled somata, 29.5% ($n = 13$) also contained DAT (Table 2), but M5R immunoreaction product was detected in nearly all (92.9%; Table 2) DAT-immunolabeled somata. In such dual-labeled somata, M5R had the same localization as in non–DAT-containing cell bodies.

The immunogold labeling for M5R was commonly seen on cytoplasmic membranes within large dendrites (>1 μm), although there was a trend toward a more plasmalemmal distribution in smaller dendrites ≤ 1 μm (Figs. 4, 5). In these dendrites, plasmalemmal M5R-immunogold particles were sometimes located on synaptic specializations (Fig. 4D,E). The major cytoplasmic distribution of M5R-immunogold labeling in dendrites was quantitatively confirmed; thus, ANOVA showed significantly higher M5R-immunogold density (mean number of gold particles per dendrite) within the cytoplasm (2.012 ± 0.366) compared with the plasma membrane density (0.718 ± 0.073) in M5R-labeled dendrites ($F_{1,14} = 11.99$, $P = 0.0038$). The prominent localization of M5R immunolabeling to the cytoplasm was, however, strongly corelated to the dendritic size (ANOVA for interaction dendritic size × immunogold subcellular distribution: $F_{1,12} = 20.587$, $P = 0.0007$), being exclusive of VTA dendrites >1 μm; in dendrites <1 μm, there were not statistically significant differences in the proportions of cytoplasmic and plasmalemmal localization of M5R-immunogold labeling (Fig. 5). Analysis of the immunogold M5R distribution in randomly sampled dendrites showed that nearly 43% of the total dendritic gold particles were in contact with the plasma membrane in small dendrites (<1 μm). A statistically significant association between dendritic size and localization of M5R immunolabeling was also confirmed by using the χ^2 test for the raw number of M5R-immunogold particles in such randomly sampled M5R-labeled dendrites ($\chi^2_1 = 141.993$, $P < 0.0001$).

The M5R-immunolabeled dendrites received multiple synaptic contacts from unlabeled axon terminals ($n = 216$, 96%; Figs. 2, 4), as well as from a few from M5R-immunoreactive terminals ($n = 9$, 4%). Symmetric

(n = 117) and asymmetric (n = 108) synapses on M5R-immunoreactive dendrites were similarly prevalent (52% vs. 48%, respectively). Statistical analysis showed that the distribution in area density of symmetric and asymmetric synapses (number of synapses of each type per analyzed unit area) did not differ significantly with respect to synapses that were formed between either unlabeled terminals (t_3 = 0.686; P = 0.542), M5R-labeled terminals (t_3 = 0.140; P = 0.897), or total axon terminals (t_3 = 0.934; P = 0.351) and M5R-immunoreactive dendrites.

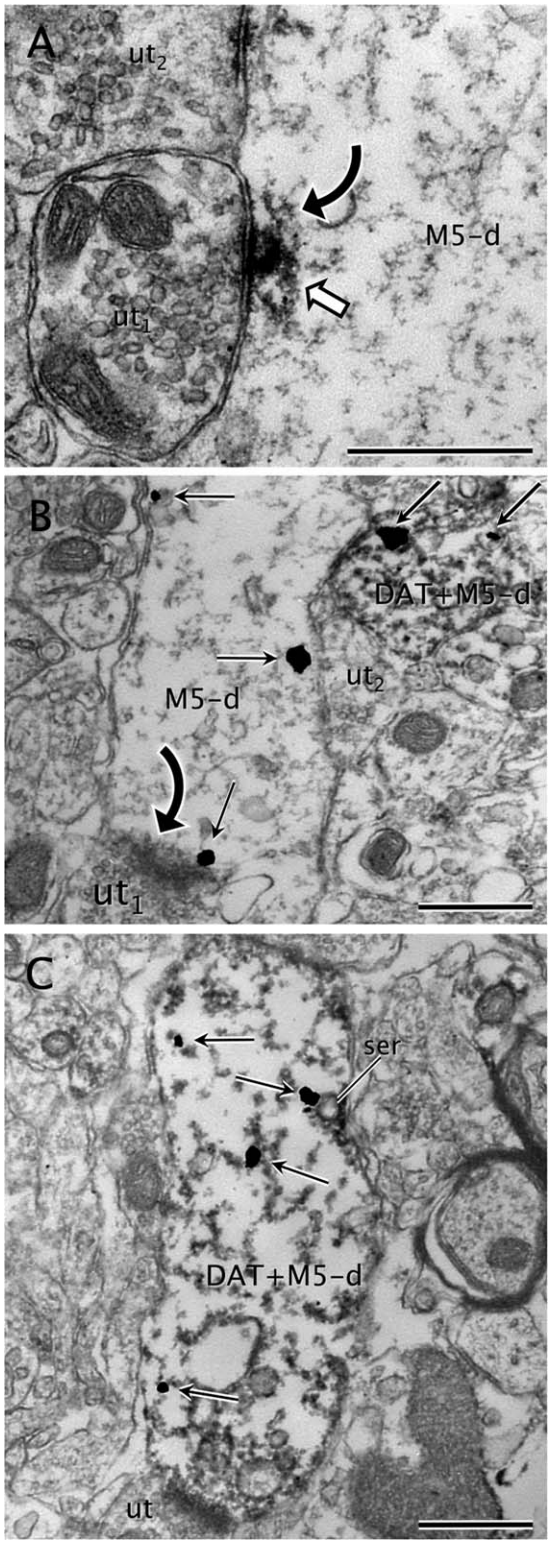

Figure 2.

M5R and DAT distributions in separate, apposed, or single dendrites

The M5R-immunoreactive dendritic profiles were scattered in a neuropil containing numerous DAT-immunolabeled somatodendritic profiles (n = 1,562 total DAT-immunoreactive profiles; Table 2). Many of these labeled dendrites were separated from each other by glial leaflets, small unmyelinated axons, and axon terminals differentially contacting either the DAT- or the M5R-labeled dendrites (Fig. 4). In some cases, however, dendrites showing differential immunolabeling had apposed plasmalemmal surfaces and were contacted by a single common afferent axon terminal (Fig. 2B). Twenty-one percent of the single M5R-labeled dendrites (n = 88 of 419) were apposed to DAT-immunoreactive dendrites (either with or without M5R), establishing a total number of 134 contacts. In these M5R-immunoreactive dendrites, the labeling did not show any perceptible difference from that present in other dendrites apposing unlabeled profiles.

DAT immunoreactivity was detected almost exclusively in dendrites (n = 1,446/1,562, 93%) whose sizes were similar to those containing M5R, according to the known existence in the VTA of abundant dopaminergic

Figure 2. M5 labeling in DAT and non-DAT labeled dendrites. **A:** Immunoperoxidase reaction product for M5 (white block arrow) is seen within a dendrite (M5-d). The labeling is located beneath an apparently symmetric synapse (curved arrow) from an unlabeled axon terminal (ut_1). M5-immunoperoxidase is also evident near the plasma membrane of M5-d in a zone near an apposition with another unlabeled axon terminal (ut_2). **B:** An M5-labeled dendrite (M5-d) showing M5-immunogold particles (straight black arrows) localized to cytoplasmic areas near the plasma membrane. Note that one M5-immunogold particle is definitely attached to the postsynaptic density on an asymmetric synapse (curved black arrow) from an unlabeled axon terminal (ut). The M5-d also contacts a dendrite (DAT+M5-d) that contains both DAT-immunoperoxidase and M5-immunogold. An unlabeled axon terminal (ut) apposes both the single M5-d and the dual DAT+M5-d. **C:** M5-immunogold particles (straight black arrows) are seen within the cytoplasm of a dendrite (M5+DAT-d) also showing intense immunoreactivity for DAT. Note that one of the M5-immunogold particles is located on tubulovesicles of smooth endoplasmic reticulum (ser). This dendrite receives a synapse from an unlabeled terminal (ut). Scale bar = 0.5 μm in A–C.

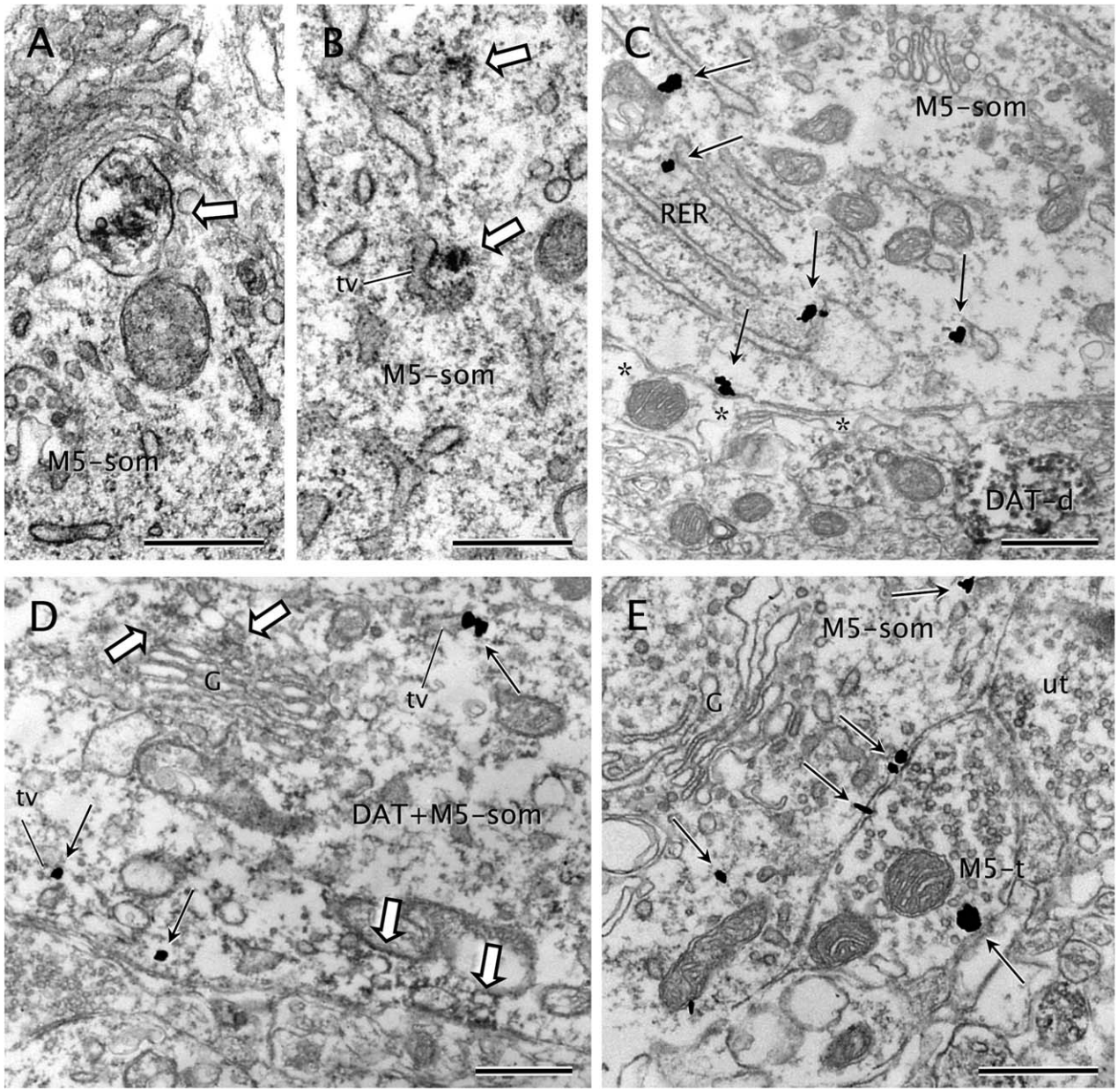

Figure 3. M5 distribution in neuronal somata. **A:** M5-immunoperoxidase (white block arrow) is seen in an endomembrane body within a soma (M5-som). **B:** M5-immunoperoxidase precipitate (white block arrows) is localized to cytoplasm and cytoplasmic tubulovesicles (tv) in a neuronal soma (M5-som). **C:** An M5-immunoreactive soma (M5-som) shows prominent M5-immunogold particles (black straight arrows) on membranes of endoplasmic reticulum cisterns (RER) and on the plasma membrane. A small dendrite intensely immunoreactive for DAT (DAT-d) is seen in the adjoining neuropil. Asterisks, astrocytic coverage. **D:** Moderate DAT-immunoperoxidase deposits (white block arrows) are present on the cytoplasmic surface of the plasma membrane or near to endomembranes of the Golgi complex (G) in a soma showing also M5-immunogold particles (black straight arrows) mainly in tubulovesicles (tv) of the endoplasmic reticulum. **E:** An M5-immunolabeled soma (M5-som) shows widespread immunogold labeling (black straight arrows) on or near portions of the plasma membrane apposing an axon terminal (M5-t). The terminal exhibits one plasmalemmal M5-immunogold particle and apposes an adjacent unlabeled terminal (ut). Scale bar = 0.5 μm in A–E.

neurons with highly branched local dendritic arborizations, but virtually no dopaminergic terminals (Fig. 4) (Nirenberg et al., 1997; Garzón et al., 1999). About one-third of the M5R-immunogold labeled dendrites (33.2%; n = 208 of 627) contained DAT-immunoperoxidase reaction product (Table 2); conversely, 14.4% of the DAT-immunolabeled dendrites showed M5R labeling (n = 208 of 1,446). M5R subcellular localization in the dual-labeled dendrites showed a similar distribution to that seen in M5R single-labeled

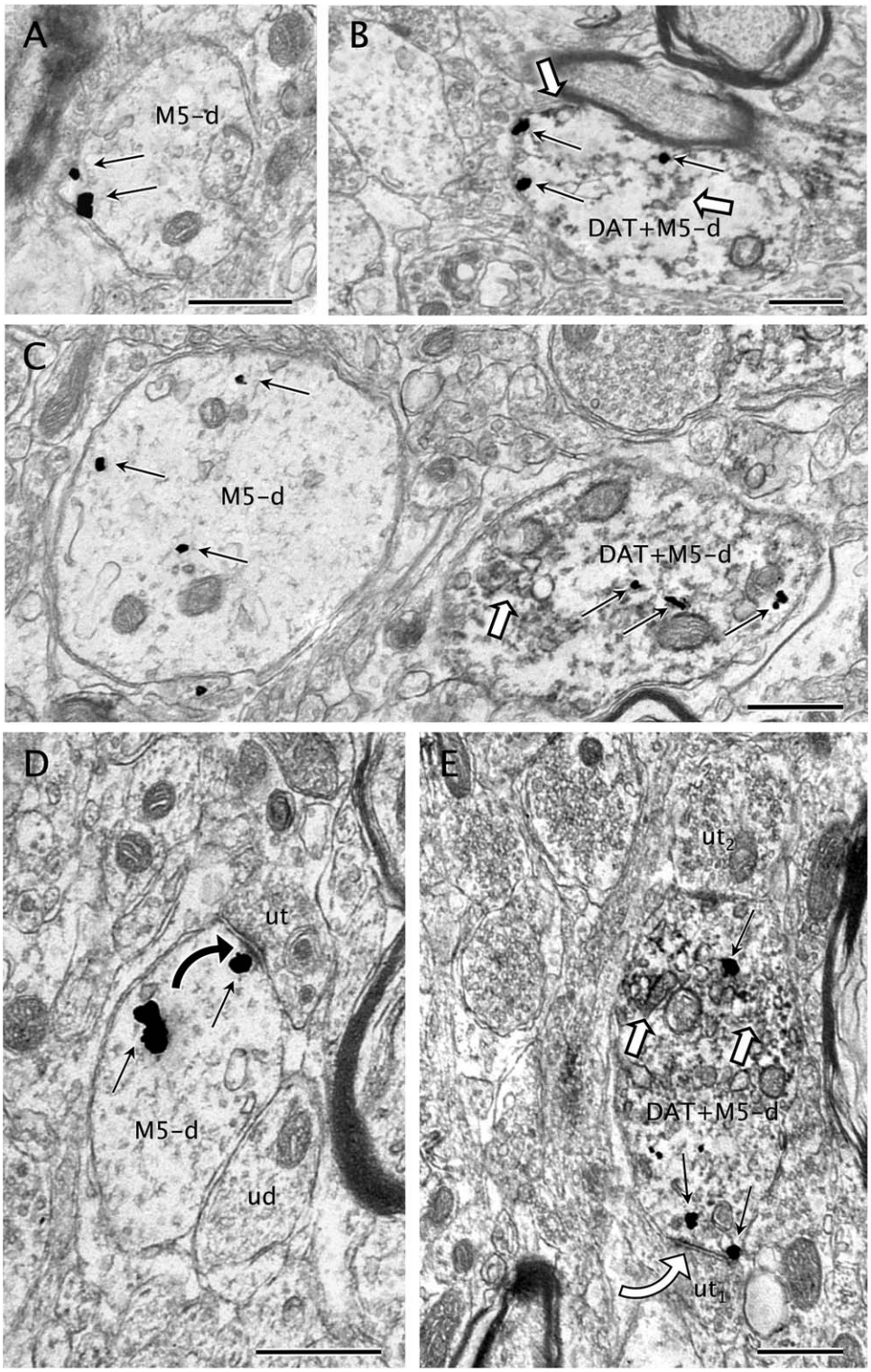

Figure 4. M5-immunogold labeling in dendrites with or without DAT. **A:** M5-immunogold particles (black straight arrows) are seen on the plasma membrane of a small dendrite devoid of DAT. **B:** A dually labeled small dendrite (DAT+M5-d) contains M5-immunogold particles (black straight arrows) mostly localized on the plasma membrane as well as immunoperoxidase reaction product for DAT (white block arrows). **C:** M5-immunogold particles (black straight arrows) are localized within the cytoplasm of a transversally sectioned large dendrite (M5-d) without expression of DAT. The dendrite is near another large dendrite (DAT+M5) that shows DAT-immunoperoxidase (white block arrow) and M5-immunogold. **D:** An unlabeled axon terminal (ut) makes an asymmetric synapse (black curved arrow) with an M5-immunogold (black straight arrows) labeled dendrite (M5-d). One of the M5-immunogold particles is located near the postsynaptic density of the established synapse. The plasmalemmal surface of M5-d is also in contact with an adjoining unlabeled dendrite (ud). **E:** A dual-labeled dendrite (DAT+M5-d) showing DAT-immunoperoxidase (white block arrows) and M5-immunogold particles (black straight arrows), one of which is localized on the postsynaptic density of an incoming symmetric synapse (white curved arrow) from an unlabeled terminal (ut1). Another unlabeled axon terminal (ut_2) also provides synaptic input to DAT+M5-d in a distant opposite portion of M5-d plasma membrane. Scale bar = 0.5 μm in A–E.

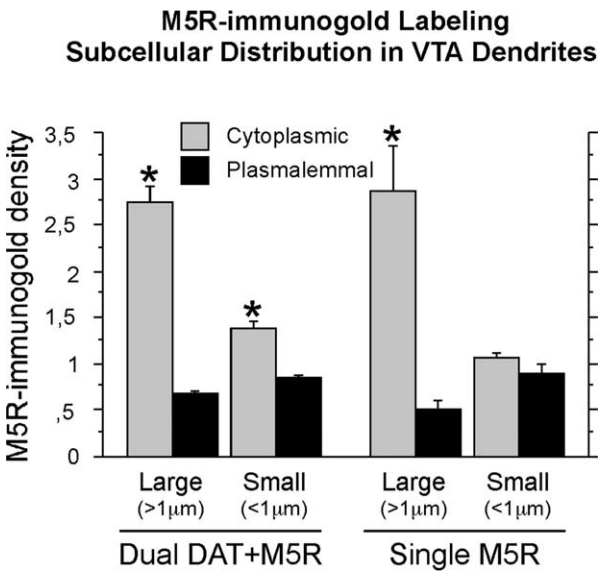

Figure 5. Bar graph summarizing the mean ± SE immunogold densities (number of gold particles per profile) in M5R-single and dopamine transporter (DAT)+M5R-dual large (>1 μm) or small (<1 μm) dendrites within the VTA. Mean densities were calculated based on the numbers obtained from 627 VTA dendrites (215 large and 412 small) taken from ultrathin sections from 14 Vibratome sections in four rats (2,288 total immunolabeled profiles) processed for dual labeling. *, $P < 0.05$, Fisher's test for cytoplasmic versus plasmalemmal subcellular localization.

dendrites (Figs. 2, 4), in that M5R-immunogold in the dual-labeled dendrites had a sparse and mostly cytoplasmic distribution (Fig. 5). Thus, two-way ANOVAs (factors: subcellular distribution × labeling type) showed statistically significant variations in the mean M5R-immunogold density not related to the type of labeling (distribution: $F_{1,28} = 25.881$, $P < 0.0001$; distribution × labeling: $F_{1,28} = 0.008$, $P = 0.9283$). Furthermore, no statistical diferences were observed in the M5R-immunogold density between single- and dual-labeled dendrites (ANOVA factor, labeling type: $F_{1,28} = 0.084$, $P = 0.7736$). However, independent ANOVA for M5R-immunogold localization in the DAT-labeled dendrites indicated that, in contrast to the M5R-immunolabeled dendrites not containing DAT, the dual-labeled DAT+M5R dendrites had significantly higher cytoplasmic versus plasmalemmal densities of M5R-immunogold irrespective of the dendritic size. Thus, this difference was seen in both large ($F_{1,6} = 121.199$, $P < 0.0001$) and small ($F_{1,6} = 40.222$, $P < 0.0007$) dendrites. Therefore, M5R+DAT dual-immunolabeled dendrites are a subpopulation of M5R-labeled dendrites in which M5R immunolabeling density in the cytoplasm is significantly higher than on the plasma membrane even in the small dendrites. This is in clear contrast to the single M5R-immunoreactive small dendrites ($F_{1,6} = 2.401$, $P = 0.1723$). Dendrites that were dual labeled for M5R and DAT received asymmetric and symmetric inputs mainly from unlabeled terminals (Figs. 2, 4).

M5R distribution in axons

Axon terminals ($n = 102$) and small unmyelinated axons ($n = 88$) containing M5R-immunogold comprised around 22% of the total M5R-labeled neuronal processes in the VTA (Table 2). M5R-qimmunolabeled unmyelinated axons were ≤0.2 μm in diameter, rarely contained small synaptic vesicles, and did not make recognizable junctions with apposing profiles. These axons were frequently observed in bundles with other unlabeled axons in the VTA neuropil (Fig. 6A). A few isolated myelinated axons ($n = 7$) also showed cytoplasmic M5R immunolabeling (Fig. 6D).

The M5R-immunoreactive terminals were morphologically heterogeneous in size (0.25–1.2 μm diameter) and synaptic specialization. These terminals contained densely packed small synaptic vesicles (40–60 nm in diameter) and sometimes one or more mitochondria (Fig. 6). The M5R-immunoperoxidase reaction product within these terminals appeared as dense homogeneous precipitates confined to discrete portions of the terminal (Fig. 6B). The labeling frequently rimmed clusters of small synaptic vesicles near the perimeter of the terminal and the cytoplasmic surface of the plasma membrane, but was usually distant from presynaptic membrane specializations (Fig. 6F). M5R-immunoperoxidase labeling was localized to vesicles and/or tubulovesicles in perisynaptic sites (Fig. 6C,E) or more distant plasmalemmal segments apposed to glial or axonal processes (Fig. 6F). Immunogold–silver labeling confirmed the cytoplasmic and plasmalemmal localization of M5R. Thus, 57.8% of the M5R immunogold-silver particles ($n = 118$) were seen in the cytoplasm. M5R immunogold–silver particles were also located primarily near or in contact with small synaptic vesicles (Fig. 7A). Because the size of the immunogold particles was usually larger than the vesicles, no attempt was made to quantify the frequency of these contacts. Gold–silver particles identifying M5R in axon terminals were, however, also detected on the plasma membranes ($n = 86$; 42.2%), sometimes in the vicinity of synaptic junctions (Fig. 7B). Almost none of the M5R-immunolabeled terminals expressed DAT immunoreactivity (Table 2).

M5R immunoreactivity in axon terminals contacting M5R- or DAT-containing dendrites

M5R-immunoreactive axon terminals often apposed astrocytic profiles (Fig. 6B,C,F), small axons (Fig. 6E,F), or other axon terminals (Fig. 6). When the M5R-labeled

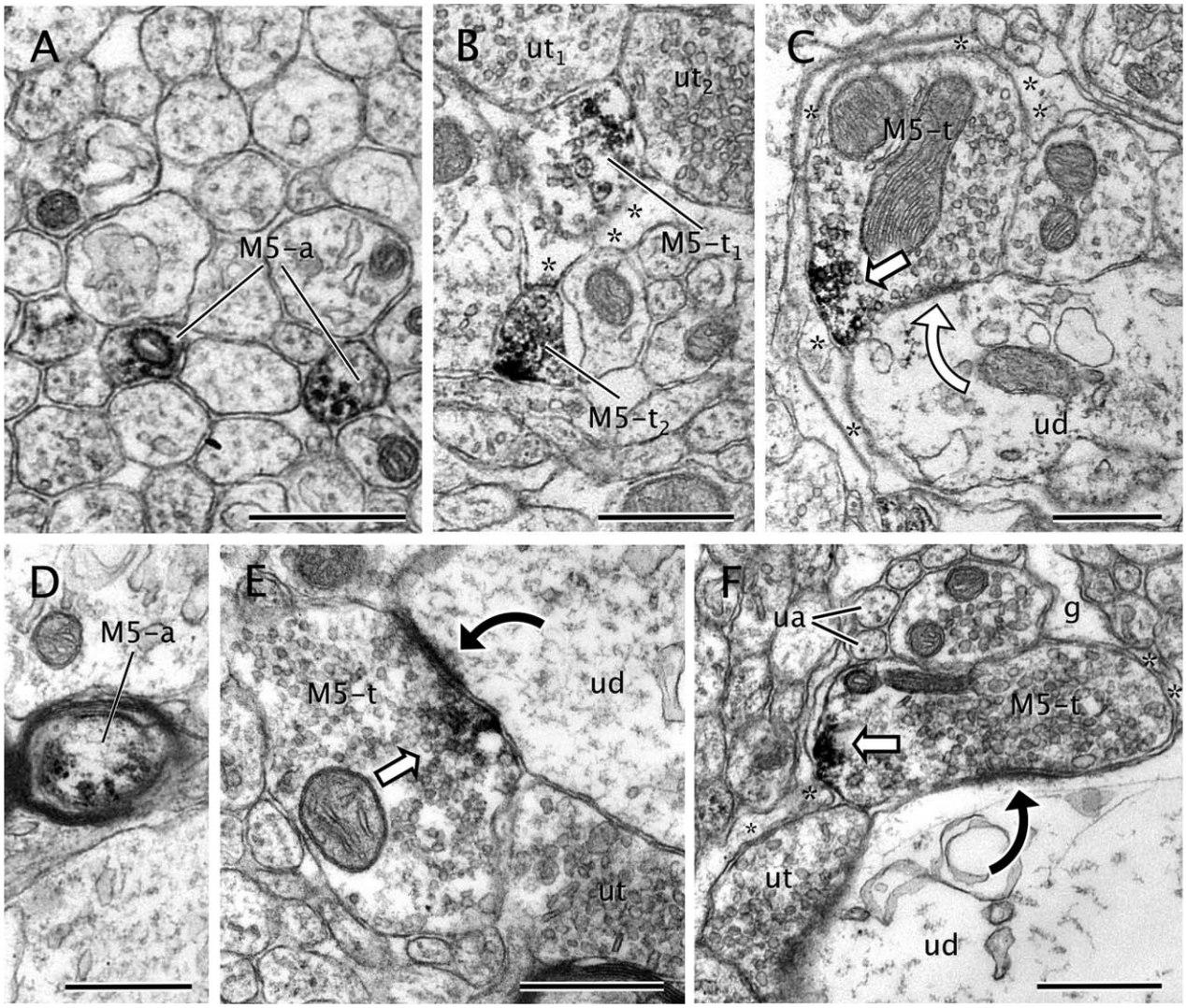

Figure 6. M5-immunolabeling in axons and axon terminals. **A:** M5-immunoperoxidase precipitate is seen within the cytoplasm of transversally sectioned small unmyelinated axons (M5-a) that traverse the neuropil forming bundles with many other unlabeled axons. **B:** Axon terminal showing a patch of immunoperoxidase labeling for M5 (M5-t_1) in small synaptic vesicles contacts two unlabeled axon terminals ($ut_{1,2}$). A more conspicuous distribution of M5-immunoperoxidase is seen on the plasma membrane of another axon terminal (M5-t_2). Asterisks indicate surrounding astrocytic processes. **C:** M5-immunoperoxidase is localized on portions of the plasma membrane in an axon terminal (M5-t). The terminal is covered by an astrocytic process (asterisk) and located near a contact with an unlabeled dendrite (ud). **D:** M5-immunoperoxidase (white block arrows) is observed on the plasma membrane and within the cytoplasm of a myelinated axon (M5-a). **E:** Axon terminal (M5-t) showing M5 immunoreactivity (white block arrow) on endomembranes and small synaptic vesicles localized near or apposed to the plasma membrane. The M5-t forms an asymmetric synapse (black curved arrow) onto an unlabeled dendrite (ud). **F:** A dense patch of M5-immunoperoxidase (white block arrow) is observed on the plasma membrane of an axon terminal (M5-t). This terminal shows extensive glial coverage (asterisks), including the zone adjacent to the M5-peroxidase reaction product. The M5-t makes an asymmetric synapse (black curved arrow) with a large unlabeled dendrite (ud). g, glia; ua, unlabeled small unmyelinated axon. Scale bar = 0.5 μm in A–F.

terminals formed synapses with dendrites, both pre- and postsynaptic elements were frequently ensheathed by a common glial process (Fig. 6C). Glial processes also frequently enclosed appositional contacts between M5R-labeled terminals and other profiles. Some of the M5R-immunoreactive terminals formed synaptic junctions with either unlabeled (n = 31) or M5R-labeled (n = 3) dendrites (Figs. 6E,F, 7A,B). The synapses established by M5R-immunoreactive terminals were either asymmetric (n = 21) or symmetric (n = 17); there were no statistically significant differences in the area density of asymmetric versus symmetric synapses within synapses established between M5R terminals and either unlabeled (t_3 = 2.438; P = 0.093) or

M5R-labeled ($t_3 = 0.154$; $P = 0.888$) dendrites. In the few cases observed with M5R localization in both the pre- and the postsynaptic elements, the M5R-immunoreactive axon terminals contained immunogold–silver particles that were distant from the contacts with the M5R-labeled dendrites.

Only 18% ($n = 18$) of the M5R-labeled terminals contacted dendrites containing DAT immunoreactivity (Fig. 7A,C) despite the high prevalence of DAT-immunolabeled dendrites within the VTA neuropil ($n = 1,446$). Most of these contacts were appositional junctions in which synaptic specializations could not be discerned in the plane of section, and only in a few cases ($n = 4$) were distinct synaptic specializations clearly observed. DAT-immunolabeled dendrites recipient to M5R-immunoreactive terminals received convergent input from unlabeled terminals, apposed small axons, or were covered by astrocytic processes, but rarely contacted other labeled or unlabeled dendrites (Fig. 7).

The M5R-immunoreactive axon terminals frequently apposed other axon terminals that did not contain immunoreactivity for either M5R or DAT (Fig. 6B); in many cases both the unlabeled and the M5R-labeled axon terminals contacted a common target dendrite (Fig. 6E,F). In these terminals M5R immunolabeling was localized on sectors of the plasma membrane distant from the unlabeled apposing terminals (Fig. 6E,F).

M5R immunolabeling in glial profiles

M5R immunoreactivity was detected in glial profiles as defined by their irregular contours and/or intermediate filaments in the VTA. However, these profiles comprised only 5.3% ($n = 50$) of the total M5R-immunoreactive processes in the VTA. Immunoperoxidase (Fig. 7E,F) labeling for M5R or immunogold–silver particles (Fig. 7C) were observed mainly along segments of glial plasma membranes. Labeled astrocytic plasma membranes often apposed or wrapped unlabeled dendrites (Fig. 7D) or terminals (Fig 7E,F). In dual-labeled tissue, glial processes labeled for M5R were not seen often in contact with DAT-labeled dendrites.

Comparison of M5R and DAT distributions

There were significant differences in the number of DAT, M5R, and DAT+M5R immunolabeled profiles per analyzed unit area (ANOVA: $F_{2,39} = 15.053$, $P < 0.001$; mean ± SEM values: DAT, 0.102 ± 0.017 profiles/μm^2; M5R, 0.055 ± 0.009 profiles/μm^2; DAT+M5R, 0.016 ± 0.003 profiles/μm^2). However, there were no statistically significant variations among different animals in the inmunolabeling area density for either of these labeled profiles (DAT, $F_{3,10} = 0.517$, $P = 0.68$; M5R, $F_{3,10} = 0.824$, $P = 0.51$; dual DAT+M5R, $F_{3,10} = 0.652$, $P = 0.60$). Nested ANOVAs also indicated statistically significant differences in the distribution of M5R immunolabeling in specific subcellular compartments (ANOVA factor, profile type: $F_{6,266} = 505.118$, $P < 0.0001$), but an absence of significant differences among animals was detected in those distributions (ANOVA profile type × animal: $F_{18,266} = 0.469$, $P = 0.9692$).

DISCUSSION

The results of the present study show for the first time ultrastructural evidence that in the rat VTA the M5R muscarinic receptor has both a plasmalemmal and endomembrane distribution extensively localized to dendrites, many of which are dopaminergic. Moreover, we demonstrate that these dendrites receive asymmetric and/or symmetric synaptic input mainly from unlabeled terminals and also appose DAT-labeled dendrites or axons. These results indicate that postsynaptic dendrites of dopaminergic neurons are major potential targets for M5R activation in the VTA. They also reveal, however, that M5R activation may occur even more frequently in distal dendrites that are either nondopaminergic or lack detectable DAT. Non–DAT-containing axons and glial profiles are also identified as potential targets for activation of the M5R. The observed distribution of M5R, together with previous findings on M2R localization, suggest a highly complex cholinergic regulation of VTA neurons through activation of multiple muscarinic receptor subtypes at distinct cellular domains in transmitter-specific neurons as well as glia. This suggests diverse modulatory mechanisms that contribute to muscarinic-induced activation of mesolimbic neurons in the VTA.

Methodological considerations

The characterization of the DAT antiserum used in this study has been previously reported (Ciliax et al., 1999). This antiserum shows a high specificity for the antigenic DAT peptide in multiple brain regions including the VTA (Ciliax et al., 1999; Svingos et al., 1999, 2001; González-Hernández et al., 2004; Garzón and Pickel, 2006). We employed DAT as a marker for DA neurons because it selectively localizes sites for DA reuptake/release and psychostimulant binding directly involved in DA-mediated reward. DAT is less sensitive than the DA-synthesizing enzyme tyrosine hydroxylase for identification of DA phenotype in mesocortical axons at the ultrastructural level (Sesack et al., 1998; Lewis et al., 2001) and this may reflect reduced somatodendritc expression of DAT in VTA mesocortical neurons

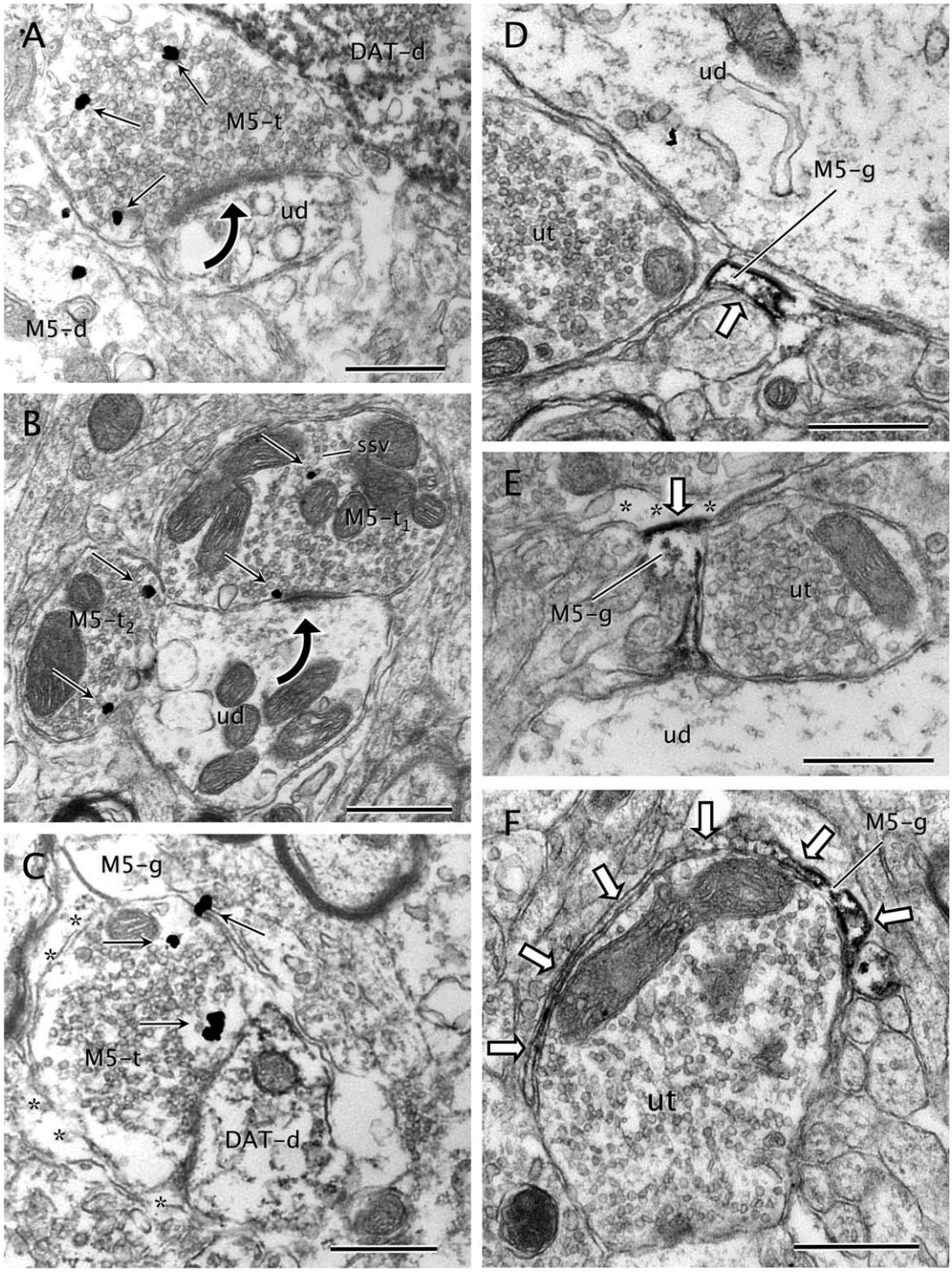

Figure 7. M5-immunogold labeling in axon terminals and glial processes. **A:** Axon terminal showing immunogold particles (black straight arrows) for M5 (M5-t) makes an asymmetric synapse (black curved arrow) with an unlabeled dendrite (ud). The terminal also apposes an intense DAT-immunoperoxidase labeled dendrite (DAT-d) and an M5-immunogold labeled dendrite (M5-d). **B:** M5-immunogold particles (black straight arrows) are localized to small synaptic vesicles (ssv) within an M5-immunolabeled terminal (M5-t_1). The M5-immunogold is also seen on the presynaptic side of an asymmetric synapse (black curved arrow) made with an unlabeled dendrite (ud). This dendrite contacts another M5-immunoreactive terminal (M5-t_2) showing both plasmalemmal and cytoplasmic M5-immunogold particles (black straight arrows). **C:** M5-immunogold particles (black straight arrows) are seen in an axon terminal (M5-t) making contact with a dendrite containing DAT-immunoperoxidase (DAT-d). The M5-t is wrapped by an astrocytic expansion showing M5-immunogold particles (M5-g) and an unlabeled astrocytic profile (asterisks). **D:** M5-immunoperoxidase reaction product (white block arrow) neatly rims the plasma membrane of an astrocytic process (M5-g). The labeled process is immersed among other unlabeled profiles (ut, unlabeled terminal; ud, unlabeled dendrite) within the neuropil. **E:** M5-immunoperoxidase is prevalently distributed on the inner surface of the plasma membrane (white block arrow) in an astrocytic profile (M5-g). A gap junction (white block arrow) is seen between the M5-g and an adjacent astrocytic process (asterisks). M5-g also apposes an unlabeled terminal (ut) and an unlabeled dendrite (ud). **F:** An astrocytic leaflet extension (M5-g) containing M5 immunolabeling (white block arrows) wraps partially around the surface of an unlabeled axon terminal (ut). Scale bar = 0.5 μm in A–F.

(Ciliax et al., 1995). However, this is not the case for mesolimbic neurons that are mainly involved in M5R-mediated actions. Also, DAT has proved to be a sensitive marker for VTA DA somata and dendrites in previous ultrastructural studies (Nirenberg et al., 1997). The M5R-immunogold labeling was located on the cytoplasmic surfaces of plasma membranes, in agreement with the recognition of the i3 intracellular loop of the human cloned M5R gene including the peptidic sequence against which the antiserum was raised (Bonner et al., 1987). Finally, specificity of M5R labeling in the present study is also supported by: 1) absence of labeling in negative control experiments with omission of the M5R antiserum; 2) background control experiments with substitution of the secondary antiserum; and 3) absence of labeling in M5R knockout mice.

Pre-embedding immunocytochemistry achieves good ultrastructural preservation of the tissue and ensures the identification of antigens that are sensitive to plastic embedding, but has limited penetration of immunoreagents (Leranth and Pickel, 1989). Thus, differential penetration of gold versus peroxidase in dual-labeling procedures may contribute to an underestimation of the number of labeled profiles and/or frequency of associations. Therefore, to achieve valuable quantitative analysis of dual labeling in sections processed before plastic embedding, and to minimize the probability of false negatives, we: 1) freeze-thawed the tissue sections to enhance penetration of immunoreagents; and 2) only collected ultrathin sections near the resin–tissue interface, which has the most complete access to immunoreagents. We also used the immunoperoxidase and immunogold–silver markers for M5R receptor detection in order to obtain more optimal information on both subcellular distribution and frequency of associations. In most cases, only a few immunogold particles were observed in neuronal profiles that were considered to be labeled for either antigen. This is a coherent approach only in samples of tissue such as those used in this study, in which structures such as myelin show few, if any, stray gold particles, and there was equivalence between the subcellular localization seen with immunogold and immunoperoxidase markers. These precautions greatly enhanced the method reliability and partially overcame its limitations. Thus, although the quantitative values may underestimate the total number of profiles containing M5R and DAT, they provide a good relative comparison of the cellular and subcellular distribution of the labeling patterns.

Somatodendritic localization of M5R

Immunogold–silver particles for M5R were readily detected in selective neuronal perikarya, inclusive of almost all somata labeled for DAT. These data are consistent with previous *in situ* hybridization studies reporting that M5 mRNA is present in large cells of midbrain dopaminergic regions (Vilaró et al., 1990; Weiner et al., 1990). Our data, however, indicate that non-DA neurons may also express M5R. The presence of M5R labeling in somata and dendrites that lack detectable DAT implies that M5R activation in the VTA may also play a role in controlling the postsynaptic activity of non-DA neurons. However, the diferential surface expression of DAT and M5R suggests that compartmentation of these proteins within DA neurons may account for the separate distributions.

The present observation of M5R localization mainly on endomembranes in somata and large dendrites suggests the participation of those organelles in the synthesis, transport, recycling, and/or internalization of the receptors from functional sites on the plasma membrane (Stowell and Craig, 1999; Achour et al., 2008). Availability of muscarinic receptors is known to be downregulated by internalization of receptors in early endosomes after binding to specific ligands (Bernard et al., 1998, 2006; van Koppen, 2001; Bendor et al., 2010; Thangaraju and Sawyer, 2011). Our results suggest, therefore, that somata are not likely to be a common site for binding of M5R agonists in the VTA given the low expression of M5R on their plasma membrane, but rather a compartment for synthesis and sorting of M5R. The cytoplasmic distribution of M5R in VTA somata thus suggests that the receptors may be in a nonfunctional reservoir compartment where they are recruitable for rapid mobilization to required activation sites on distal dendrites. Also, cytoplasmic M5R localization may denote trafficking to terminal fields in cortical and limbic territories, where M5R activation modulates presynaptic transmitter release (Vannucchi and Pepeu, 1995; Yeomans, 2012). Abundant evidence exists for presynaptic M5R-mediated DA release in striatal terminals of VTA neurons (Yamada et al., 2001; Kuroiwa et al., 2012; Zhang et al., 2012b), and mechanisms have been described for activity-induced M5R endocytic recycling in those terminals (Bendor et al., 2010). Recent data suggest that this M5R-mediated presynaptic DA release depends not only on receptor activation in NAc mesolimbic DA axon terminals, but mainly on M4-type muscarinic receptors located on NAc cholinergic interneurons, which autoregulate acetylcholine release and subsequent cholinergic signaling (Liste et al., 2003; Threlfell et al., 2010). To our knowledge, M5R activation in cortical DA axons has not yet been reported.

M5R distribution on plasma membranes of dendrites suggests rapid activation after acute occupation by

ligands (Xu et al., 2007). Furthermore, M5R activation in the VTA is necessary to produce the tonic excitation and prolonged mesolimbic NAc DA release that sustains rewarding brain stimulation and motivational behaviors (Yeomans et al., 2001; Forster et al., 2002; Miller and Blaha, 2005). Our observation of higher plasmalemmal M5R localization in dendritic profiles that did not express DAT suggests that nondopaminergic neurons, most probably γ-aminobutyric acid (GABA)ergic (Steffensen et al., 1998), are also a potential target for M5R activation in the VTA. Similar results on a higher trend for plasmalemmal versus cytoplasmic localization in distal dendrites of non-DA neurons have been described previously for the M2R subtype (Garzón and Pickel, 2006). The GABAergic neurons in the VTA comprise local circuit neurons and projection neurons of the mesocorticolimbic pathway (Van Bockstaele and Pickel, 1995; Steffensen et al., 1998; Carr and Sesack, 2000). Thus, a postsynaptic action mediated through M5R in these neurons could significantly affect the activity of VTA neurons as well as their cortical and limbic targets. Alternatively, however, we cannot exclude the possibility that small distal dendrites have a more limited dendritic release of DA and therefore less demand for expression levels of DAT, even though small dendrites are known to express both DAT and tyrosine hydroxylase (Nirenberg et al., 1997; Pickel et al., 2002).

Axonal localization of M5R

The observation of M5R labeling mainly in non-DA axonal profiles that make asymmetric or symmetric synapses in the VTA is consistent with a primary involvement of M5R in the release of, respectively, excitatory (Grillner et al., 1999; Grillner and Mercuri, 2002) or inhibitory (Grillner et al., 2000; Michel et al., 2004; González et al., 2011) neurotransmitters other than DA in this region. Although both actions are assumed to involve preferentially muscarinic receptors of the subtype M3, a subsidiary M5R participation could not be excluded because of the lack of M5R-selective antagonists (Grillner and Mercuri, 2002; Michel et al., 2004). The VTA is enriched in glutamate-containing axons originating in the cerebral cortex and numerous subcortical structures (Parent et al., 1999; Geisler et al., 2007) including the mesopontine cholinergic nuclei (Charara et al., 1996; Smith et al., 1996), as well as in intrinsic VTA glutamatergic neurons (Dobi et al., 2010). Similarly, striatal and pallidal neurons provide the VTA with abundant GABA terminals (Bayer and Pickel, 1991; Sesack and Pickel, 1995), whose inhibitory action could be increased by M5R activation of GABA terminals present in the VTA. Overall, our data suggest that M5Rs are putative sites for the alleged presynaptic muscarinic-mediated activation of excitatory glutamate or inhibitory GABA inputs modulating the postsynaptic excitability of VTA neurons (Miller and Blaha, 2005). Also, because cholinergic axon terminals have a strong excitatory drive within the VTA (Lacey et al., 1990; Blaha et al., 1996; 1999), we cannot exclude the possibility that some of our M5R-labeled terminals belong to mesopontine cholinergic neurons involved in mesocorticolimbic activation (Garzón and Pickel, 2000; Yeomans, 1995, 2012).

Glial localization of M5R

Localization of muscarinic receptors to glial cells has been previously described (for review, see Porter and McCarthy, 1997). No definitive clue is available yet as to the specific muscarinic receptor subtypes present in glial cells in the VTA, although a previous study showed a subtle M2R immunolabeling (Garzón and Pickel, 2006). In hippocampal slices, muscarinic activation increases intracellular calcium concentration in astrocytes in situ that is blocked by the muscarinic antagonist pirenzepine (Shelton and McCarthy, 2000; Araque et al., 2002). Because, in addition to M1R, pirenzepine antagonizes, albeit with lesser power, all muscarinic $G\alpha_{q/11}$-coupled receptors (M1/M3/M5) (Augelli-Szafran et al., 1999), a role for M5R in intracellular calcium mobilization resulting from neuronal–glial communication can be hypothesized.

Functional implications

The present results provide new insights into the subcellular sites responsible for M5R-mediated control of mesocorticolimbic reward behaviors (Yeomans et al., 2000, 2001; Basile et al., 2002; Zhang et al., 2002a; Yamada et al., 2003; Fink-Jensen et al., 2003; Thomsen et al., 2005, 2007; Liu et al., 2007a; Steidl and Yeomans, 2009; Schmidt et al., 2010). Our findings are consistent with VTA M5R involvement in both natural- and drug-rewarding behaviors, most likely by stimulating mesolimbic DA release (Forster et al., 2002; Yamada et al., 2003). M5R inactivation attenuates reward and withdrawal manifestations to opioids (Basile et al., 2002; Miller et al., 2005; Liu et al., 2007a; Steidl and Yeomans, 2009; Steidl et al., 2011) or cocaine (Fink-Jensen et al., 2003; Thomsen et al., 2005; Lester et al., 2010).

In addition, our demonstration of M5R targeting to DAT-containing dendrites of the VTA may help substantiate the proposed implication of M5R in schizophrenia (Wang et al., 2004). Interference with M5R activation in VTA dopaminergic neurons accounts for the decreased prepulse inhibition observed in M5R-deficient mice (Thomsen et al., 2007). Together, these data support

the well-known antipsychotic effects of some muscarinic drugs. Furthermore, direct haplotype analysis evidence exists linking M5R and schizophrenia (De Luca et al., 2004).

CONFLICT OF INTEREST STATEMENT

The authors declare that they have no conflict of interest.

ROLE OF AUTHORS

Both authors had full access to all the data in the study and take responsibility for the integrity of the data and the accuracy of the data analysis. Both authors contributed equally to the design and implementation of the experiments as well as manuscript preparation. The first author (MG) is largely responsible for collection of images and data analysis.

LITERATURE CITED

Achour L, Labbé-Jullié C, Scott MGH, Marullo S. 2007. An escort for GPCRs: implications for regulation of receptor density at the cell surface. Trends Pharmacol Sci 29:528–533.

Alderson HL, Latimer MP, Blaha CD, Phillips AG, Winn P. 2004. An examination of d-amphetamine self-administration in pedunculopontine tegmental nucleus-lesioned rats. Neuroscience 125:349–358.

Araque A, Martín ED, Perea G, Arellano JI, Buño W. 2002. Synaptically released acetylcholine evokes Ca^{2+} elevations in astrocytes in hippocampal slices. J Neurosci 22:2443–2450.

Augelli-Szafran CE, Blankley CJ, Jaen JC, Moreland DW, Nelson CB, Penvose-Yi JR, Schwarz RD, Thomas AJ. 1999. Identification and characterization of m1 selective muscarinic receptor antagonists1. J Med Chem 42:356–363.

Basile AS, Fedorova I, Zapata A, Liu X, Shippenberg T, Duttaroy A, Yamada M, Wess J. 2002. Deletion of the M5 muscarinic acetylcholine receptor attenuates morphine reinforcement and withdrawal but not morphine analgesia. Proc Natl Acad Sci U S A 99:11452–11457.

Bayer VE, Pickel VM. 1991. GABA-labeled terminals form proportionally more synapses with dopaminergic neurons containing low densities of tyrosine hydroxylase-immunoreactivity in rat ventral tegmental area. Brain Res 559:44–55.

Bendor J, Lizardi-Ortiz JE, Westphalen RI, Brandstetter M, Hemmings HD Jr, Sulzer D, Flajolet M, Greengard P. 2010. AGAP1/AP-3-dependent endocytic recycling of M5 muscarinic receptors promotes dopamine release. EMBO J 29:2813–2826.

Bernard V, Laribi O, Levey AI, Bloch B. 1998. Subcellular redistribution of m2 muscarinic acetylcholine receptors in striatal interneurons in vivo after acute cholinergic stimulation. J Neurosci 18:10207–10218.

Bernard V, Décossas M, Liste I, Bloch B. 2006. Intraneuronal trafficking of G-protein-coupled receptors in vivo. Trends Neurosci 29:140–147.

Blaha CD, Allen LF, Das S, Inglis WL, Latimer MP, Vincent SR, Winn P. 1996. Modulation of dopamine efflux in the nucleus accumbens after cholinergic stimulation of the ventral tegmental area in intact, pedunculopontine tegmental nucleus-lesioned, and laterodorsal tegmental nucleus-lesioned rats. J Neurosci 16:714–722.

Bonner TI, Buckley NJ, Young AC, Brann MR. 1987. Identification of a family of muscarinic acetylcholine receptor genes. Science 237:527–532.

Bonner TI, Young AC, Brann MR, Buckley NJ. 1988. Cloning and expression of the human and rat m5 muscarinic acetylcholine receptor genes. Neuron 1:403–410.

Bymaster FP, Shannon HE, Rasmussen K, Delapp NW, Mitch CH, Ward JS, Calligaro DO, Ludvigsen TS, Sheardown MJ, Olesen PH, Swedberg MD, Sauerberg P, Fink-Jensen A. 1998. Unexpected antipsychotic-like activity with the muscarinic receptor ligand (5R,6R)6-(3-propylthio-1,2,5-thiadiazol-4-yl)-1-azabicyclo[3.2.1]octane. Eur J Pharmacol 356:109–119.

Bymaster FP, McKinzie DL, Felder CC, Wess J. 2003. Use of M1-M5 muscarinic receptor knockout mice as novel tools to delineate the physiological roles of the muscarinic cholinergic system. Neurochem Res 28:437–442.

Carr DB, Sesack SR. 2000. GABA-containing neurons in the rat ventral tegmental area project to the prefrontal cortex. Synapse 38:114–123.

Chan J, Aoki C, Pickel VM. 1990. Optimization of differential immunogold-silver and peroxidase labeling with maintenance of ultrastructure in brain sections before plastic embedding. J Neurosci Methods 33:113–127.

Charara A, Smith Y, Parent A. 1996. Glutamatergic inputs from the pedunculopontine nucleus to midbrain dopaminergic neurons in primates: *Phaseolus vulgaris*-leucoagglutinin anterograde labeling combined with postembedding glutamate and GABA immunohistochemistry. J Comp Neurol 364:254–266.

Ciliax BJ, Heilman C, Demchyshyn LL, Pristupa ZB, Ince E, Hersch SM, Niznik HB, Levey AI. 1995. The dopamine transporter: immunocytochemical characterization and localization in brain. J Neurosci 15:1714–1723.

Ciliax BJ, Drash GW, Staley JK, Haber S, Mobley CJ, Miller GW, Mufson EJ, Mash DC, Levey AI. 1999. Immunocytochemical localization of the dopamine transporter in human brain. J Comp Neurol 409:38–56.

De Luca V, Wang H, Squassina A, Wong GW, Yeomans J, Kennedy JL. 2004. Linkage of M5 muscarinic and alpha7-nicotinic receptor genes on 15q13 to schizophrenia. Neuropsychobiology 50:124–127.

Dobi A, Margolis EB, Wang HL, Harvey BK, Morales M. 2010. Glutamatergic and nonglutamatergic neurons of the ventral tegmental area establish local synaptic contacts with dopaminergic and nondopaminergic neurons. J Neurosci 30:218–229.

Eldred WD, Zucker C, Karten HJ, Yazulla S. 1983. Comparison of fixation and penetration enhancement techniques for use in ultrastructural immunocytochemistry. J Histochem Cytochem 31:285–292.

Fink-Jensen A, Kristensen P, Shannon HE, Calligaro DO, Delapp NW, Whitesitt C, Ward JS, Thomsen C, Rasmusseen T, Sheardown MJ, Jeppesen L, Sauerberg P, Bymaster FP. 1998. Muscarinic agonists exhibit functional dopamine antagonism in unilaterally 6- OHDA lesioned rats. Neuroreport 9:3481–3486.

Fink-Jensen A, Fedorova I, Wörtwein G, Woldbye DP, Rasmussen T, Thomsen M, Bolwig TG, Knitowski KM, McKinzie DL, Yamada M, Wess J, Basile A. 2003. Role for M5 muscarinic acetylcholine receptors in cocaine addiction. J Neurosci Res 74:91–96.

Forster GL, Blaha CD. 2000. Laterodorsal tegmental stimulation elicits dopamine efflux in the rat nucleus accumbens by activation of acetylcholine and glutamate receptors in the ventral tegmental area. Eur J Neurosci 12:3596–3604.

Forster GL, Yeomans JS, Takeuchi J, Blaha CD. 2002. M5 muscarinic receptors are required for prolonged accumbal dopamine release after electrical stimulation of the pons in mice. J Neurosci 22:RC190.

Garzón M, Pickel VM. 2000. Dendritic and axonal targeting of the vesicular acetylcholine transporter to membranous cytoplasmic organelles in laterodorsal and pedunculopontine tegmental nuclei. J Comp Neurol 419:32–48.

Garzón M, Pickel VM. 2006. Subcellular distribution of M2 muscarinic receptors in relation to dopaminergic neurons of the rat ventral tegmental area. J Comp Neurol 498:821–839.

Garzón M, Vaughan RA, Uhl GR, Kuhar MJ, Pickel VM. 1999. Cholinergic axon terminals in the ventral tegmental area target a subpopulation of neurons expressing low levels of the dopamine transporter. J Comp Neurol 410:197–210.

Geisler S, Derst C, Veh RW, Zahm DS. 2007. Glutamatergic afferents of the ventral tegmental area in the rat. J Neurosci 27:5730–5743.

Giros B, Jaber M, Jones SR, Wightman RM, Caron MG. 1996. Hyperlocomotion and indifference to cocaine and amphetamine in mice lacking the dopamine transporter. Nature 379:606–612.

González JC, Albiñana E, Baldelli P, García AG, Hernández-Guijo JM. 2011. Presynaptic muscarinic receptor subtypes involved in the enhancement of spontaneous GABAergic postsynaptic currents in hippocampal neurons. Eur J Neurosci 33:69–81.

González-Hernández T, Barroso-Chinea P, De La Cruz Muros I, Del Mar Pérez-Delgado M, Rodríguez M. 2004. Expression of dopamine and vesicular monoamine transporters and differential vulnerability of mesostriatal dopaminergic neurons. J Comp Neurol 479:198–215.

Gray EG. 1959. Axosomatic and axo-dendritic synapses of the cerebral cortex: an electron microscopic study. J Anat 93:420–433.

Grillner P, Mercuri NB. 2002. Intrinsic membrane properties and synaptic inputs regulating the firing activity of the dopamine neurons. Behav Brain Res 130:149–169.

Grillner P, Bonci A, Svensson TH, Bernardi G, Mercuri NB. 1999. Presynaptic muscarinic (M3) receptors reduce excitatory transmission in dopamine neurons of the rat mesencephalon. Neuroscience 91:557–565.

Grillner P, Berretta N, Bernardi G, Svensson TH, Mercuri NB. 2000. Muscarinic receptors depress GABAergic synaptic transmission in rat midbrain dopamine neurons. Neuroscience 96:299–307.

Gronier B, Rasmussen K. 1998. Activation of midbrain presumed dopaminergic neurones by muscarinic cholinergic receptors: an *in vivo* electrophysiological study in the rat. Br J Pharmacol 124:455–464.

Gronier B, Perry KW, Rasmussen K. 2000. Activation of the mesocorticolimbic dopaminergic system by stimulation of muscarinic cholinergic receptors in the ventral tegmental area. Psychopharmacology 147:347–355.

Henderson Z, Sherriff FE. 1991. Distribution of choline acetyltransferase immunoreactive axons and terminals in the rat and ferret brainstem. J Comp Neurol 314:147–163.

Hersch SM, Yi H, Heilman CJ, Edwards RH, Levey AI. 1997. Subcellular localization and molecular topology of the dopamine transporter in the striatum and substantia nigra. J Comp Neurol 388:211–227.

Hsu SM, Raine L, Fanger H. 1981. The use of avidin-biotin-peroxidase complex (ABC) in immunoperoxidase technique: a comparison between ABC and unlabeled antibody (peroxidase) procedures. J Histochem Cytochem 29:577–599.

Ikemoto S, Wise RA. 2002. Rewarding effects of the cholinergic agents carbachol and neostigmine in the posterior ventral tegmental area. J Neurosci 22:9895–9904.

Kubo T, Fukuda K, Mikami A, Maeda A, Takahashi H, Mishina M, Haga T, Haga K, Ichiyama A, Kangawa K, Kojima M, Matsuo H, Hirose T, Numa S. 1986. Cloning, sequencing and expression of complementary DNA encoding the muscarinic acetylcholine receptor. Nature 323:411–416.

Kuhar MJ, Ritz MC, Boja JW. 1991. The dopamine hypothesis of the reinforcing properties of cocaine. Trends Neurosci 14:299–302.

Kuroiwa M, Hamada M, Hieda E, Shuto T, Sotogaku N, Flajolet M, Snyder GL, Hendrick JP, Fienberg A, Nishi A. 2012. Muscarinic receptors acting at pre- and post-synaptic sites differentially regulate dopamine/DARPP-32 signaling in striatonigral and striatopallidal neurons. Neuropharmacology 63:1248–1257.

Lacey MG, Calabresi P, North RA. 1990. Muscarine depolarizes rat substantia nigra zona compacta and ventral tegmental neurons in vitro through M_1-like receptors. J Pharmacol Exp Ther 253:395–400.

Leranth C, Pickel VM. 1989. Electron microscopic pre-embedding double immnunostaining methods. In: Heimer L, Zaborsky L, editors. Tract tracing methods. Vol 2, Recent progress. New York: Plenum. p 129–172.

Lester DB, Miller AD, Blaha CD. 2010. Muscarinic receptor blockade in the ventral tegmental area attenuates cocaine enhancement of laterodorsal tegmentum stimulation-evoked accumbens dopamine efflux in the mouse. Synapse 64:216–223.

Levey AI, Kitt CA, Simonds WF, Price DL, Brann MR. 1991. Identification and localization of muscarinic acetylcholine receptor proteins in brain with subtype-specific antibodies. J Neurosci 11:3218–3226.

Lewis DA, Melchitzky DS, Sesack SR, Whitehead RE, Auh S, Sampson A. 2001. Dopamine transporter immunoreactivity in monkey cerebral cortex: regional, laminar, and ultrastructural localization. J Comp Neurol 432:119–136.

Liao CF, Themmen AP, Joho R, Barberis C, Birnbaumer M, Birnbaumer L. 1989. Molecular cloning and expression of a fifth muscarinic acetylcholine receptor. J Biol Chem 264:7328–7337.

Liste I, Bernard V, Bloch B. 2002. Acute and chronic acetylcholinesterase inhibition regulates in vivo the localization and abundance of muscarinic receptors m2 and m4 at the cell surface and in the cytoplasm of striatal neurons. Mol Cell Neurosci 20:244–256.

Liu HF, Zhou WH, Zhu HQ, Lai MJ, Chen WS. 2007a. Microinjection of M(5) muscarinic receptor antisense oligonucleotide into VTA inhibits FosB expression in the NAc and the hippocampus of heroin sensitized rats. Neurosci Bull 23:1–8.

Liu Q, Wu J, Wang X, Zeng J. 2007b. Changes in muscarinic acetylcholine receptor expression in form deprivation myopia in guinea pigs. Mol Vis 13:1234–1244.

Mark GP, Shabani S, Dobbs LK, Hansen ST. 2011. Cholinergic modulation of mesolimbic dopamine function and reward. Physiol Behav 104:76–81.

Michel FJ, Robillard JM, Trudeau LE. 2004. Regulation of rat mesencephalic GABAergic neurones through muscarinic receptors. J Physiol 556:429–445.

Miller AD, Blaha CD. 2005. Midbrain muscarinic receptor mechanisms underlying regulation of mesoaccumbens and nigrostriatal dopaminergic transmission in the rat. Eur J Neurosci 21:1837–1846.

Miller AD, Forster GL, Yeomans JS, Blaha CD. 2005. Midbrain muscarinic receptors modulate morphine-induced

accumbal and striatal dopamine efflux in the rat. Neuroscience 136:531–538.

Miller GW, Staley JK, Heilman CJ, Perez JT, Mash DC, Rye DB, Levey AI. 1997. Immunochemical analysis of dopamine transporter protein in Parkinson's disease. Ann Neurol 41:530–539.

Nirenberg MJ, Chan J, Vaughan RA, Uhl G, Kuhar MJ, Pickel VM. 1997. Immunogold localization of the dopamine transporter: an ultrastructural study of the rat ventral tegmental area. J Neurosci 17:4037–4044.

Oakman SA, Faris PL, Kerr PE, Cozzari C, Hartman BK. 1995. Distribution of pontomesencephalic cholinergic neurons projecting to substantia nigra differs significantly from those projecting to ventral tegmental area. J Neurosci 15:5859–5869.

Olmstead MC, Munn EM, Franklin KB, Wise RA. 1998. Effects of pedunculopontine tegmental nucleus lesions on responding for intravenous heroin under different schedules of reinforcement. J Neurosci 18:5035–5044.

Omelchenko N, Sesack SR. 2005. Laterodorsal tegmental projections to identified cell populations in the rat ventral tegmental area. J Comp Neurol 483:217–235.

Omelchenko N, Sesack SR. 2006. Cholinergic axons in the rat ventral tegmental area synapse preferentially onto mesoaccumbens dopamine neurons. J Comp Neurol 494:863–875.

Parent A, Parent M, Charara A. 1999. Glutamatergic inputs to midbrain dopaminergic neurons in primates. Parkinsonism Relat Disord 5:193–201.

Paxinos G, Watson C. 1986. The rat brain in stereotaxic coordinates. San Diego: Academic Press.

Peralta EG, Winslow JW, Peterson GL, Smith DH, Ashkenazi A, Ramachandran J, Schimerlik MI, Capon DJ. 1987. Primary structure and biochemical properties of an M2 muscarinic receptor. Science 236:600–605.

Peters A, Palay SL, Webster HD. 1991. The fine structure of the nervous system: neurons and their supporting cells. New York: Oxford University Press.

Pickel VM, Garzón M, Mengual E. 2002. Electron microscopic immunolabeling of transporters and receptors identifies transmitter-specific functional sites envisioned in Cajal's neuron. Prog Brain Res 136:145–55.

Porter JT, McCarthy KD. 1997. Astrocytic neurotransmitter receptors in situ and in vivo. Prog Neurobiol 51:439–55.

Pristupa ZB, Wilson JM, Hoffman BJ, Kish SJ, Niznik HB. 1994. Pharmacological heterogeneity of the cloned and native human dopamine transporter: disassociation of [^{3}H]WIN 35,428 and [^{3}H]GBR 12,935 binding. Mol Pharmacol 45:125–135.

Qu J, Zhou X, Xie R, Zhang L, Hu D, Li H, Lu F. 2006. The presence of m1 to m5 receptors in human sclera: evidence of the sclera as a potential site of action for muscarinic receptor antagonists. Curr Eye Res 31:587–97.

Reynolds ES. 1963. The use of lead citrate at high pH as an electron-opaque stain in electron microscopy. J Cell Biol 17:208.

Schmidt LS, Miller AD, Lester DB, Bay-Richter C, Schülein C, Frikke-Schmidt H, Wess J, Blaha CD, Woldbye DP, Fink-Jensen A, Wortwein G. 2010. Increased amphetamine-induced locomotor activity, sensitization, and accumbal dopamine release in M5 muscarinic receptor knockout mice. Psychopharmacology (Berl) 207:547–558.

Sesack SR, Pickel VM. 1995. Ultrastructural relationships between terminals immunoreactive for enkephalin, GABA, or both transmitters in the rat ventral tegmental area. Brain Res 672:261–275.

Sesack SR, Hawrylak VA, Matus C, Guido MA, Levey AI. 1998. Dopamine axon varicosities in the prelimbic division of the rat prefrontal cortex exhibit sparse immunoreactivity for the dopamine transporter. J Neurosci 18:2697–2708.

Shelton MK, McCarthy KD. 2000. Hippocampal astrocytes exhibit Ca^{2+}-elevating muscarinic cholinergic and histaminergic receptors in situ. J Neurochem 74:555–563.

Smith Y, Charara A, Parent A. 1996. Synaptic innervation of midbrain dopaminergic neurons by glutamate-enriched terminals in the squirrel monkey. J Comp Neurol 364:231–253.

Steffensen SC, Svingos AL, Pickel VM, Henriksen SJ. 1998. Electrophysiological characterization of GABAergic neurons in the ventral tegmental area. J Neurosci 18:8003–8015.

Steidl S, Yeomans JS. 2009. M5 muscarinic receptor knockout mice show reduced morphine-induced locomotion but increased locomotion after cholinergic antagonism in the ventral tegmental area. J Pharmacol Exp Ther 328:263–275.

Steidl S, Miller AD, Blaha CD, Yeomans JS. 2011. M5 muscarinic receptors mediate striatal dopamine activation by ventral tegmental morphine and pedunculopontine stimulation in mice. PLoS One 6:e27538.

Stowell JN, Craig AM. 1999. Axon/dendrite targeting of metabotropic glutamate receptors by their cytoplasmic carboxy-terminal domains. Neuron 22:525–536.

Svingos AL, Clarke CL, Pickel VM. 1999. Localization of the delta-opioid receptor and dopamine transporter in the nucleus accumbens shell: implications for opiate and psychostimulant cross-sensitization. Synapse 34:1–10.

Svingos AL, Chavkin C, Colago EE, Pickel VM. 2001. Major coexpression of kappa-opioid receptors and the dopamine transporter in nucleus accumbens axonal profiles. Synapse 42:185–192.

Thangaraju A, Sawyer GW. 2011. Comparison of the kinetics and extent of muscarinic M1-M5 receptor internalization, recycling and downregulation in Chinese hamster ovary cells. Eur J Pharmacol 650:534–543.

Thomsen M, Woldbye DP, Wörtwein G, Fink-Jensen A, Wess J, Caine SB. 2005. Reduced cocaine self-administration in muscarinic M5 acetylcholine receptor-deficient mice. J Neurosci 25:8141–8149.

Thomsen M, Wörtwein G, Fink-Jensen A, Woldbye DP, Wess J, Caine SB. 2007. Decreased prepulse inhibition and increased sensitivity to muscarinic, but not dopaminergic drugs in M5 muscarinic acetylcholine receptor knockout mice. Psychopharmacology (Berl) 192:97–110.

Threlfell S, Clements MA, Khodai T, Pienaar IS, Exley R, Wess J, Cragg SJ. 2010. Striatal muscarinic receptors promote activity dependence of dopamine transmission via distinct receptor subtypes on cholinergic interneurons in ventral versus dorsal striatum. J Neurosci 30:3398–3408.

Van Bockstaele EJ, Pickel VM. 1995. GABA-containing neurons in the ventral tegmental area project to the nucleus accumbens in rat brain. Brain Res 682:215–221.

van Koppen CJ. 2001. Multiple pathways for the dynamin-regulated internalization of muscarinic acetylcholine receptors. Biochem Soc Trans 29:505–508.

Vannucchi MG, Pepeu G. 1995. Muscarinic receptor modulation of acetylcholine release from rat cerebral cortex and hippocampus. Neurosci Lett 190:53–56.

Vilaró MT, Palacios JM, Mengod G. 1990. Localization of m5 muscarinic receptor mRNA in rat brain examined by in situ hybridization histochemistry. Neurosci Lett 114:154–159.

Wang H, Ng K, Hayes D, Gao X, Forster G, Blaha C, Yeomans J. 2004. Decreased amphetamine-induced locomotion and improved latent inhibition in mice mutant for the M5 muscarinic receptor gene found in the human

15q schizophrenia region. Neuropsychopharmacology 29:2126–2139.

Weiner DM, Levey AI, Brann MR. 1990. Expression of muscarinic acetylcholine and dopamine receptor mRNAs in rat basal ganglia. Proc Natl Acad Sci U S A 87:7050–7054.

Wess J. 2003. Novel insights into muscarinic acetylcholine receptor function using gene targeting technology. Trends Pharmacol Sci 24:414–420.

Westerink BHC, Kwint H-F, De Vries JB. 1996. The pharmacology of mesolimbic dopamine neurons: a dual-probe microdialysis study in the ventral tegmental area and nucleus accumbens of the rat brain. J Neurosci 16:2605–2611.

Xu ZQ, Zhang X, Scott L. 2007. Regulation of G protein-coupled receptor trafficking. Acta Physiol (Oxf) 190:39–45.

Yamada M, Lamping KG, Duttaroy A, Zhang W, Cui Y, Bymaster FP, McKinzie DL, Felder CC, Deng CX, Faraci FM, Wess J. 2001. Cholinergic dilation of cerebral blood vessels is abolished in M(5) muscarinic acetylcholine receptor knockout mice. Proc Natl Acad Sci U S A 98:14096–14101.

Yamada M, Basile AS, Fedorova I, Zhang W, Duttaroy A, Cui Y, Lamping KG, Faraci FM, Deng CX, Wess J. 2003. Novel insights into M5 muscarinic acetylcholine receptor function by the use of gene targeting technology. Life Sci 74:345–353.

Yeomans JS. 1995. Role of tegmental cholinergic neurons in dopaminergic activation, antimuscarinic psychosis and schizophrenia. Neuropsychopharmacology 12:3–16.

Yeomans JS. 2012. Muscarinic receptors in brain stem and mesopontine cholinergic arousal functions. Handb Exp Pharmacol 208:243–259.

Yeomans J, Baptista M. 1997. Both nicotinic and muscarinic receptors in ventral tegmental area contribute to brain-stimulation reward. Pharmacol Biochem Behav 57:915–921.

Yeomans JS, Mathur A, Tampakeras M. 1993. Rewarding brain stimulation: role of tegmental cholinergic neurons that activate dopamine neurons. Behav Neurosci 107:1077–1087.

Yeomans JS, Takeuchi J, Baptista M, Flynn DD, Lepik K, Nobrega J, Fulton J, Ralph MR. 2000. Brain-stimulation reward thresholds raised by an antisense oligonucleotide for the M5 muscarinic receptor infused near dopamine cells. J Neurosci 20:8861–8867.

Yeomans J, Forster G, Blaha C. 2001. M5 muscarinic receptors are needed for slow activation of dopamine neurons and for rewarding brain stimulation. Life Sci 68:2449–2456.

You ZB, Wang B, Zitzman D, Wise RA. 2008. Acetylcholine release in the mesocorticolimbic dopamine system during cocaine seeking: conditioned and unconditioned contributions to reward and motivation. J Neurosci 28:9021–9029.

Zhang W, Basile AS, Gomeza J, Volpicelli LA, Levey AI, Wess J. 2002a. Characterization of central inhibitory muscarinic autoreceptors by the use of muscarinic acetylcholine receptor knock-out mice. J Neurosci 22:1709–1717.

Zhang W, Yamada M, Gomeza J, Basile AS, Wess J. 2002b. Multiple muscarinic acetylcholine receptor subtypes modulate striatal dopamine release, as studied with M1-M5 muscarinic receptor knock-out mice. J Neurosci 22:6347–6352.

Zhou W, Liu H, Zhang F, Tang S, Zhu H, Lai M, Kalivas PW. 2007. Role of acetylcholine transmission in nucleus accumbens and ventral tegmental area in heroin-seeking induced by conditioned cues. Neuroscience 144:1209–1218.